TRISO SiC Failure Probability for Reactivity Initiated Accidents in High-Temperature Gas-Cooled Reactors

Carlotta G. Ghezzi[1], Robert F. Kile[1], Nicholas R. Brown[1,*]

[1] University of Tennessee – Knoxville, Knoxville, TN 37902, United States

* Corresponding author: nbrown49@utk.edu

Manuscript Draft

May 13, 2022

Abstract

This work analyzes the failure process of the Silicon Carbide layer in TRISO during Reactivity Initiated Accident (RIA) scenarios for a High-Temperature Gas-Cooled reactor with BISON. Two cases are considered: a group Control Rod Withdrawal (CRW) and a Control Rod Ejection (CRE) reproduced from a previous study. Failure probability is modeled using Weibull statistics and worst-case scenario Weibull parameters are adopted to simulate the envelopes in BISON with a 1D TRISO model. CRW scenarios result as being characterized by higher values of maximum energy deposition, final temperature and volumetric strain with respect to CRE ones, but the latter have remarkably higher SiC failure probability, mainly due

to the offset in strain rates between the two cases. This work also confirms the validity and conservatism of the performance envelopes produced in a previous work by replicating the envelope formulation using RELAP5-3D and RAVEN with a different sampling technique and obtaining consistent results. A sensitivity analysis using Sobol variance decomposition method on SiC failure probability is then performed involving a set of inputs on both CRW and CRE. The two most important parameters are Weibull modulus and characteristic stress, and their relative importance depends on the specific case. The proposed interpretation of the results is that both energy deposition and strain rate influence the relative degree of importance of failure parameters. Computation of 95 % confidence intervals around worst-case scenario SiC failure probability values is also carried out for four different sets of Weibull parameters. A new criterion for SiC TRISO quality classification built upon safety-based ranges of Weibull parameters is proposed to be integrated in future Fuel-Production Quality Assurance Plans (FPQAPs).
Keywords: TRISO; BISON; HTGR; Silicon Carbide; Safety.

I. Introduction

TRistructural ISOtropic (TRISO) fuel was principally developed for High-Temperature Gas-cooled Reactors (HTGRs), though it is being considered for adaption to other reactor types due to the enhanced accident tolerance provided by its solid structure [1]. This type of fuel consists of a spherical fissile kernel which is surrounded by a low-density carbon buffer, followed by a dense Inner Pyrolytic Carbon (IPyC) coating, a Silicon Carbide (SiC) layer, and a subsequent dense Outer Pyrolytic Carbon (OPyC) coating. Among the listed constituents, SiC acts as the main barrier for the fission products that are not retained in the kernel, hence it represents a key factor during failure analysis of TRISO.

This study has as a principal objective the analysis and definition of a perimeter of challenging conditions for TRISO SiC layer that can be obtained by combining the investigation of the effects of both microscopic attributes such as SiC failure-dictating material properties and macroscopic aspects related to transient condition features. Such an analysis involves the advantageous coupling between the system-level code RELAP5-3D [2] and the fuel performance code BISON [3], which are necessary to perform a thorough safety assessment of TRISO SiC layer mechanical performance during transient conditions. The analysis conducted in this research specifically provides a contribution to delineate future TRISO safety limits expressed in terms of SiC material properties which can robustly withstand the aforementioned challenging transient conditions and prevent fission products release.

In particular, the goal of this work is to investigate the failure behavior of SiC in TRISO using BISON models for a set of Reactivity-Initiated Accident (RIA) scenarios for a graphite moderated High Temperature Reactor (HTR). Although an HTGR is considered as the example system in this study, some of the conclusions are expected to be relevant for other reactor types, such as the Fluoride salt-cooled High temperature Reactor (FHR). RIAs are characterized by insertions of positive reactivity within a reactor system, with a subsequent increase in power and temperature of the fuel, which could lead to failure [4]. These events result in thermal expansion and stress buildup [5] for the fuel particles, which can lead to the cracking of the coating layers and thus to the impairment of the fuel structural integrity. Two different RIA scenarios have been selected for this study. The first is a Design Basis Accident (DBA): a group Control Rod Withdrawal (CRW). The second is a Beyond Design Basis Accident (BDBA): a Control Rod Ejection (CRE). Both kinds of occurrences have been previously studied in depth [6] and modeled by Gorton and Brown [7] and will be reviewed in greater detail in this paper. Previous analyses performed on pulsed-power tests [5, 8], which occur over a time range on the order of milliseconds, show a direct proportionality between energy deposition in the fuel and SiC failure probability predictions by BISON for energy deposition values between 578 J/g and 1869 J/g. The RIAs this work focuses on are characterized by overall lower energy depositions, reaching a maximum of about 400 J/g, that occur over a longer time scale compared to experiments analyzed in Ref. [5] and [8], but they are more representative of RIAs in HTRs.

We focus on understanding whether failure probability predictions obtained with BISON can be considered dependent on, or proportional to, specific features of the examined transients such as energy deposition, temperature, and energy deposition rate. A secondary aspect of this research is the quantitative assessment of the relative importance of a set of parameters on BISON SiC failure probability predictions. Subsequently, we aim at quantifying the degree of uncertainty around worst-case scenario failure probability predictions for the examined scenarios by computing 95 % confidence intervals for such quantity. Conclusively, we also provide a foundation for establishing safety limits for SiC in TRISO based on the analysis of the involved accident scenarios for HTGRs. All these objectives are original contributions to the literature.

II. Background

II.A Review of HTGR accident simulations

The BISON simulations that have been performed for this work, as mentioned previously, refer to two distinct types of RIAs: a CRW and a CRE. The formulation of such realistic HTGR scenarios was first carried out by Cleveland [6]. These events have been modeled using RELAP5-3D [2] and RAVEN [9] based on a previous study by Gorton and Brown [7]. The RELAP/RAVEN models were used to generate boundary conditions for BISON. The RELAP models descend from a benchmark model for the General Atomics mHTGR-350 [10-15] The parameter ranges and distributions used with RAVEN were those from Gorton and Brown [7].

The CRW is initiated by removing three control rods from the core at a speed of 3 cm/s and the overall duration of the withdrawal is on the order of 260 s. In the sensitivity analysis conducted by Gorton and Brown [7], a set of parameters were varied over pre-determined ranges and their relative impact on a group of target variables were assessed using Sobol variance decomposition method. The input parameters that were included in the sensitivity study were the delayed neutron fraction to neutron generation time ratio, total reactivity insertion, reactivity feedback coefficients, thermal conductivities, and volumetric heat capacities. The latter three types of variables were varied for both fuel and moderator. Input variation domains were established based on a selection of rationales, including parameter changes between Beginning Of Cycle (BOC) and End Of Cycle (EOC), experimental uncertainties, and thermal and irradiation dependence of material properties. Target outputs include maximum fuel temperature, energy deposition, fuel heating rate, and peak power. Envelopes for such variables were obtained by varying the previously listed parameters and they are of key interest for this research. Figure 1 shows the obtained envelope for power as a function of time.

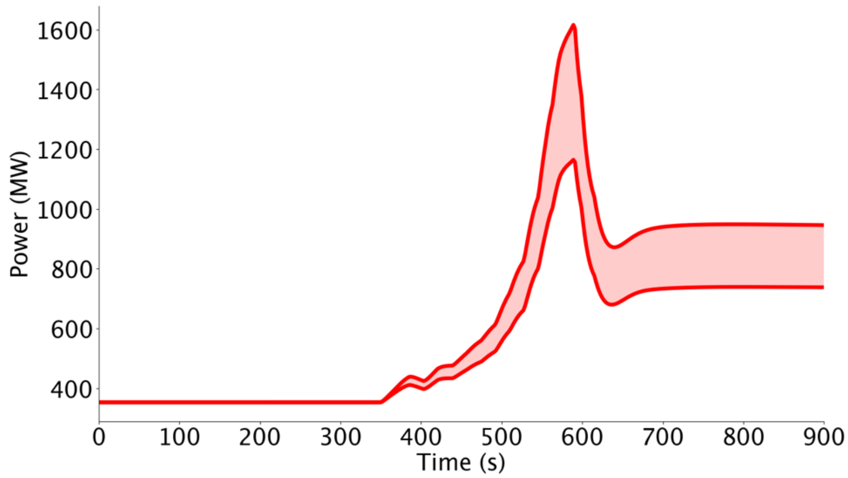

Figure 1: CRW total power envelope, data reproduced from ref. [7].

The second analyzed case was a CRE, which occurs over a much shorter timescale compared to the CRW (one second versus tens of seconds). The analysis conducted for the CRE by Gorton and Brown [7] was analogous to the one carried out for the CRW in terms of target variables, input parameters, and respective ranges. The sole exception was the case of total reactivity insertion, which was varied over a reduced range compared to CRW due to CRE involving a single control rod. The result in terms of power envelope is shown in Figure 2. Comparing Figure 1 to Figure 2 it is possible to visually assess the difference in terms of time to reach peak power between the two cases, which is an aspect that could be expected to have an impact on fuel behavior.

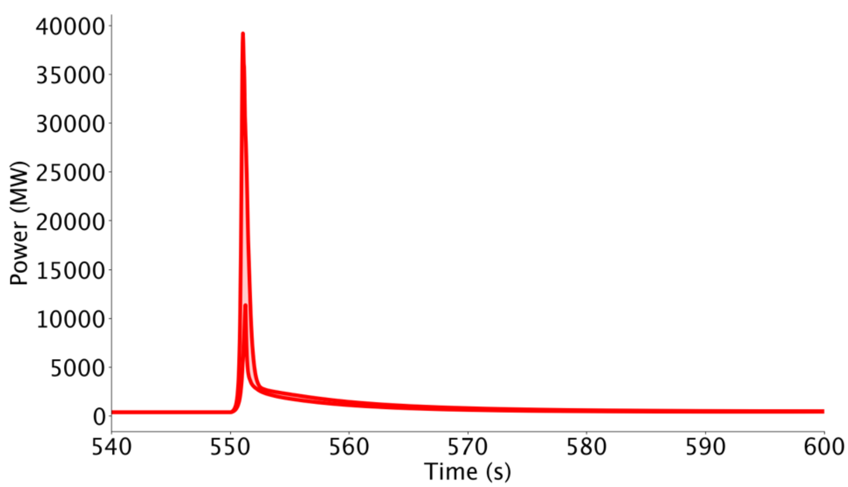

Figure 2: CRE total power envelope, data reproduced from ref. [7].

For both CRW and CRE scenarios, the same envelope of results was used to inform BISON simulations. Additional information on the previously conducted sensitivity study, parameter ranges selection, and Sobol sensitivity indices can be found in Ref. [7].

II.B RELAP5-3D model description

RELAP5-3D is a systems-level safety analysis code capable of thermal hydraulics modeling and point kinetics calculations. The RELAP model used in this analysis descends from the OECD-NEA mHTGR-350 benchmark for prismatic block reactors [10]. The mHTGR-350 is a prismatic block type reactor with hexagonal blocks containing fuel compacts and coolant channels. These hexagonal blocks are arranged into rings between an inner and outer reflector, creating an annular core design. The active core is bounded above and below by graphite reflectors as well. The RELAP model of the mHTGR-350 represents the inside of the reactor vessel, including coolant flow from the inlet to outlet, bypass channels through the core, and heat structures representing the fuel and moderator blocks. The graphite blocks in the core are modeled as a set of concentric graphite rings; three of those rings contained fuel compacts, which were modeled as a volume-fraction-weighted mixture of graphite and TRISO particles at a 35 percent packing fraction [10]. For additional information on the RELAP model, we recommend readers to Ref. [10].

The RELAP model was used to generate boundary conditions for the BISON analysis. The primary boundary conditions were peak fuel temperature and curves of power vs time.

II.C BISON model description

BISON is a fuel performance finite element code, based upon the Multiphysics Object-Oriented Simulation Environment (MOOSE) framework, that has been developed by the Idaho National Laboratory (INL) [3, 16]. Both 1D and multidimensional analysis of TRISO using BISON have been explored in previous studies for steady state and transient conditions [3, 5, 17].

For this work, a 1D model for a single TRISO particle embedded in a 40-μm graphite matrix and containing a UO_2 fuel kernel was developed. The choice of UO_2 for the kernels was carried out in order to obtain results that could be systematically compared to analogous available studies [5, 8]. One-dimensionality was adopted with the underlying assumed absence of defects related to sphericity or thickness of the layers. The geometric features for the modeled particles are the same adopted in previous studies that focused on transients in the Nuclear Safety Research Reactor (NSRR) [4]. The reason for this selection lies in the possibility to perform a subsequent systematic comparison among results obtained with BISON for this work and for preceding studies while reducing the output offset that might be due to difference in dimensions. To understand the possible impact of geometric characteristics on BISON outputs of interest, the sensitivity analysis that is part of this study also includes variables such as SiC thickness. Table *I* lists the adopted values for densities and dimensions for the modeled coated particles.

Table I: Thicknesses and densities for the modeled TRISO layers [4].

Material	**Thickness (μm)**	**Density ($g \cdot cm^{-3}$)**
UO_2	500 (diameter)	10.63
Buffer	95	1.05
IPyC	40	1.85
SiC	35	≥ 3.19
OPyC	40	1.85

The thermal properties for the TRISO layers such as specific heat, thermal conductivity, and coefficient of thermal expansion are modeled as temperature dependent in BISON and based on correlations that have been covered thoroughly in Ref. [5] and [16].

III. Methodology

III.A Best-estimate analysis with worst case properties

The simulations performed in the first part of this research are aimed at understanding what the worst-case scenarios in terms of SiC failure probability would be for the modeled accident envelopes. To this end, mechanical properties for the layers were kept constant during simulations because a temperature-dependent behavior would allow for a stress relaxation at higher temperatures which would, in turn, lower SiC failure probability predictions. Additionally, elastic moduli of TRISO layers have been proven not have a strong impact on failure probability predictions [8]. Moreover, the SiC stress-free temperature, which influences the regime at which thermal stresses shift from compressive to tensile in the material, was set to 1573 K. The reason for the selection is that such value constitutes a lower bound for deposition temperatures in TRISO CVD SiC manufacturing processes [18]. Table *II* catalogues elastic moduli and Poisson's ratios for the TRISO layers and matrix [19].

Table II: Mechanical properties for the modeled TRISO layers.

Material	**Elastic modulus (Gpa)**	**Poisson's ratio (-)**
UO_2	170	0.345
Buffer	7	0.3
PyC	29	0.3
SiC	430	0.18
Matrix	10	0.3

SiC failure probability was modeled using Weibull statistics, which has been identified as an appropriate form to describe fracture statistics behavior of brittle materials [20]. In the case of SiC spherical shells, which are the geometrical type of interest for this work, cumulative failure probability can be expressed as a function of the stress state as follows:

$$F_p = 1 - \exp\left[-\int \frac{\sum_i \sigma_{pi}^m dV}{V_c \sigma_0^m}\right] \tag{1}$$

The term σ_{pi} represents the tensile stress that SiC is subject to along the ith principal direction. Principal stresses are computed by BISON. An integration is performed over the entire volume of the specimen for which failure probability is being calculated. Three additional terms are present in Equation (1): m, σ_0 and V_c. These parameters are defined as Weibull modulus, characteristic stress, and characteristic volume, respectively, and they need to be provided as BISON model inputs. Their values can be assessed through various fracture tests with different types of specimens [18, 19, 21-23]. Due to the scatter among the data pertaining to diverse types of experiments and geometries, the adopted Weibull parameters for the current analysis were selected from a batch of tests characterized by a consistent methodology applied to only hemispherical SiC shells [23, 24] . Additional information on experimental settings and procedures can be found in Ref. [22]. While V_c is the actual volume of the specimen that has been employed to determine a given set of m and σ_0, the latter two variables are directly proportional to the relative strength of the SiC sample [20]. A SiC sample characterized by a small value of m is expected to be subject to a faster crack propagation, which is the main mechanism by which brittle materials come to failure. Moreover, a low characteristic stress is indicative of inability to withstand a stress state that is significantly higher than σ_0 itself. Such concepts have been confirmed through a sensitivity analysis performed in a previous study [8] performed on TRISO SiC failure probability and Weibull parameters. As previously stated, the first simulations performed in this analysis are focused on worst-case scenarios in terms of SiC failure probability for both CRW and CRE, which requires an appropriate choice of both Weibull modulus and characteristic stress to represent a relatively weak SiC TRISO layer. Table *III* displays the selected values for Weibull parameters, which refer to lower limits for experimentally determined m and σ_0 for hemispherical specimens [23].

Table III: Weibull parameters values for envelopes BISON simulations.

$\boldsymbol{m}\ (-)$	$\boldsymbol{\sigma_0}\ (\boldsymbol{MPa})$	$\boldsymbol{V_c}\ (-)$
3	350	$1.5 \cdot 10^{-11}$

To reproduce both CRW and CRE, a set of three RELAP outputs were adapted, properly scaled, and used as boundary conditions for BISON. Specifically, normalized reactor total power and homogenized fuel temperature. The homogenization refers to the fact that in the RELAP model used in the study by Gorton and Brown [7] the fuel was modeled as a homogenous mixture of the graphite matrix and TRISO particles with a 35% packing fraction.

III.B Sensitivity analysis

The second goal of this work is the quantitative assessment of the influence of a set of parameters on SiC failure probability variations for both CRW and CRE scenarios. From the available envelopes, which comprise 1818 cases for CRW and 1126 for CRE, two cases were selected corresponding to the highest and lowest BISON SiC failure probability predictions respectively. A total of four cases were subject to a variance-based sensitivity analysis.

Specifically, sensitivity indices were computed using Sobol decomposition method, which is categorized as a global method since it allows for a complete span of input parameters over their entire domains and thus for a thorough model output variation analysis [25]. The main benefit of Sobol method lies in its applicability to nonlinear and nonmonotonic models, as well as its ability to compute the influence of single or multiple inputs with their relative interactions on the uncertainty of the output. Detailed theoretical descriptions of sensitivity analysis methods can be found in Ref. [26-28].

Given a multi-input model f, the output Y can be expressed as follows:

$$Y = f(X_1, X_2, \dots, X_N) \tag{2}$$

Where N is the number of inputs variables. Sobol indices can be divided into two categories: first order and higher order indices respectively. For what concerns the first order terms, a main effect $S_{1,j}$ and a total effect $S_{T,j}$ Sobol indices can be defined for a given input X_j. They represent the contribution of a specific input X_j to the variance of the output: while the main effect Sobol index accounts for the impact of the input X_j alone, the total effect Sobol index also includes the contribution of the interactions between X_j and all other inputs.

$$S_{1,j} = \frac{Var[E(Y|X_j]}{Var(Y)} \tag{3}$$

$$S_{T,j} = \frac{E\left[Var\left(Y|X_{\sim j}\right)\right]}{Var(Y)} \tag{4}$$

In this work second order indices have been considered in order to examine the effect of mutual interactions between two inputs on the variance of the model output Y. Given two distinct inputs X_j and X_i, the second order Sobol index $S_{2,ji}$ can be defined as:

$$S_{2,ji} = \frac{E\left[Var\left(Y|X_j\, X_i\right)\right]}{Var(Y)} - S_{1,j} - S_{1,i} \tag{5}$$

A complete discussion on Sobol variance decomposition method is provided in Ref. [25, 29].

The Sensitivity Analysis Library (SALib) available in Python [30] has been used in this research for both parameters sampling and Sobol indices computation. The input sampling is based on an algorithm developed by Saltelli, which allows for capturing better the interactions between multiple inputs [31, 32]. Sampling is performed for each selected parameter; BISON inputs are generated using a Python script and then simulations are carried out. Subsequently, BISON output files are postprocessed using an additional Python script that computes Sobol sensitivity indices. An in-depth description of such approach is provided in detail in Refs. [33, 34].

III.C Parameters ranges

In this work, SiC failure probability represents the target for the Sobol sensitivity analysis; thus the parameters that have been chosen as variable inputs are expected to have an influence on either Weibull statistics behavior or SiC internal stress development during the transient. Table IV lists the selected parameters along with their respective ranges. In this part of the analysis, all the involved parameters are assumed as uniformly distributed within their respective ranges. The choice of a uniform distribution, along with Saltelli sampling technique [26] guarantee a thorough evaluation of the inputs domains. In Table IV, the terms ρ_{SiC}, r_{SiC} and $T_{SF,SiC}$ refer to SiC density, thickness and stress-free temperature, respectively.

Table IV: Ranges for the selected input parameters to be varied in the sensitivity analysis.

Parameter	Lower Bound	Upper Bound	Reason
$m\ (-)$	3	15	Multiple crush testing results [24, 35]
$\sigma_0\ (MPa)$	350	2450	Multiple crush testing results [24, 35]
$V_c\ (m^3)$	$4 \cdot 10^{-11}$	$1.55 \cdot 10^{-10}$	Specimen dimensional variations [18, 22, 24]
$\rho_{SiC}\ (g \cdot cm^{-3})$	3.1	3.2	TRISO manufacture uncertainties [36]
$r_{SiC}\ (\mu m)$	25	40	TRISO manufacture types [36]
$T_{SF,SiC}\ (K)$	1573	1873	Deposition temperature ranges for SiC in TRISO [36]

IV. Results

IV.A Initial Results

A total of 1818 scenarios obtained in the study by Gorton and Brown [7] for the group CRW were evaluated with the previously described 1D TRISO BISON model. The total duration of the simulations for the considered case was 900 s, of which 350 s were ran at steady state and a 1 s timestep was used. Any further timestep refinement did not yield any significant change in terms of simulation outputs. Figure 3, Figure 7 and Figure 8 show the obtained BISON envelopes for power density, maximum fuel kernel temperature and fuel volumetric expansion during the transients.

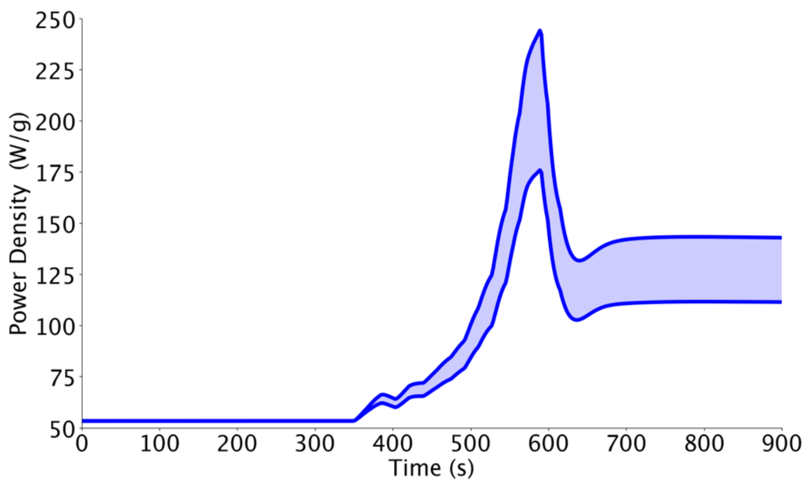

Figure 3: Power density range obtained for the CRW envelope obtained with BISON.

As it can be visually assessed comparing Figure 1 to Figure 3, no functional distortion is being introduced during BISON simulations in terms of relative power trend, with the transient starting at 350 s and power restabilizing around 700 s. For fuel volume variation depicted in Figure 8, a behavior of pure thermal expansion is found. The value for maximum energy deposition and maximum fuel temperature from BISON have been compared to those obtained with RELAP by Gorton and Brown [7] and can be found in Table *V*. The main remark about the obtained results is that BISON provides higher predictions with respect to RELAP both in terms of energy deposition and fuel maximum temperature. One of the factors that could partially explain the underlined dissimilarities is the different approximations that have been adopted in the two models. While the provided RELAP temperature is relative to a homogenized fuel which includes a graphite matrix and a 35%-packed TRISO population, the BISON prediction is indicative of the of the TRISO fuel kernel only. This difference might also have an impact on energy deposition results since the material properties utilized in the RELAP model are relative to a homogenous mixture and thus they are calculated by volume weighting the various thermal properties for the fuel constituents, whereas the calculated energy deposition from BISON is related to the TRISO fuel kernel properties alone. It is also important to underline that the BISON temperature output refers specifically to the center of the fuel kernel and that it can be found that the thermal gradient across the whole particle can reach values between approximately 10 and 20 K. An instance of the just mentioned temperature variation extending to about 20 K can be found in Figure 4, where a radial temperature profile at the end of the transient is provided for the highest temperature scenario for the CRW envelope. Given the difference between the two modeling approaches and approximations, the results obtained with BISON were considered to be in good agreement with those found by Gorton and Brown [7].

For SiC failure probability the minimum predicted value was 1.14 % and the maximum value resulting from this analysis was 12.88 %. These failure probability bounds were obtained in a worst-case scenario framework using a set of Weibull parameters that was selected among the experimental results available in literature to maximize failure probability predictions. The adopted Weibull parameters, as already mentioned in previous sections, are thus symptomatic of a defective SiC layer and the obtained failure probability envelope maximum value might reduce if different values of Weibull parameters were to be employed.

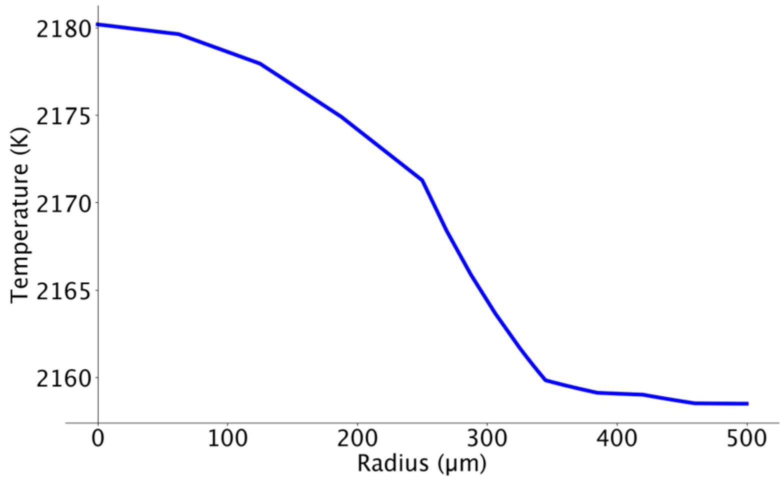

Figure 4: Radial temperature profile for the highest temperature scenario in the CRW envelope obtained with BISON.

In the case of the CRE envelope, 1126 cases were ran using the previously described 1D TRISO BISON model. The total duration was 1150 s, with the transient starting approximately at 550 s. Simulation timesteps were first set to 1.5 s and progressively reduced to an adaptable minimum allowed value of 5 ms in order to properly capture the time scale of parameters variation during the transient. The maximum allowed timestep was 25 ms. Figure 5 displays the obtained outputs in terms of peak fuel temperature for a variety of selected timesteps and it can be inferred that a value equal or above 0.5 s would likely lead to temperature underestimation for the given case.

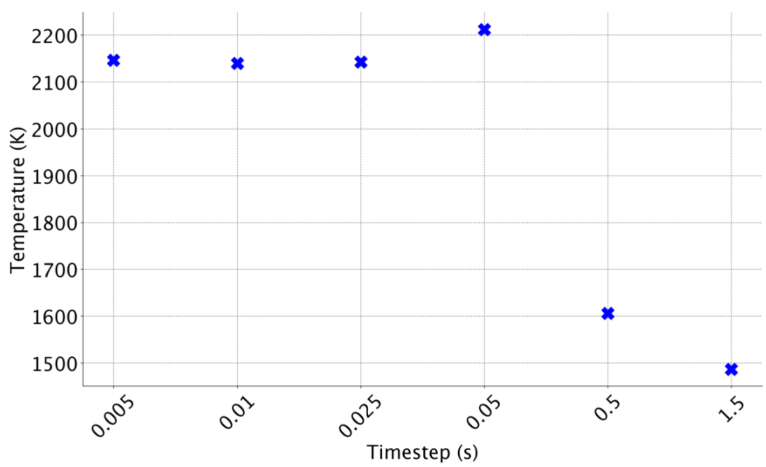

Figure 5: Peak fuel temperature as a function of the timestep for a CRE scenario.

Figure 6, Figure 7 and Figure 8 show the results that have been obtained propagating the CRE envelope by Gorton and Brown with BISON. Figure 6 shows the predicted power density envelope, which is characterized by an almost imperceptible width due to the short duration of each transient, which is on the order of one second or less. It can also be inferred comparing Figure 6 to Figure 3 that the maximum power density reached in the CRE scenarios is more than one order of magnitude higher than the one observed for the CRW cases, and that peak power is reached in a time frame that is about two orders of magnitudes shorter for CRE. Figure 7 displays the maximum kernel temperature trend as a function of time for the analyzed cases. As the transient begins, temperature immediately reaches a peak value and then it re-stabilizes as power reduces. The fuel volume envelope as a function of time is shown in Figure 8 and it can be observed that, as for the CRW case, the volumetric variations obey a thermal expansion behavior.

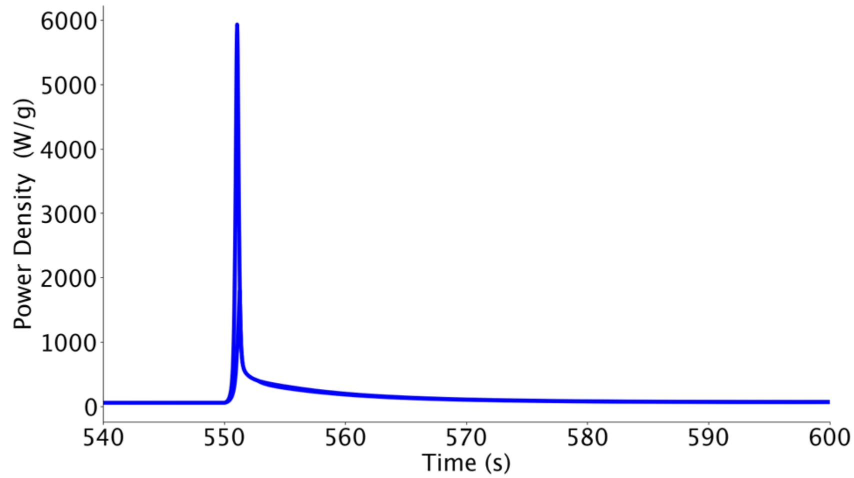

Figure 6: Power density range obtained for the CRE envelope obtained with BISON.

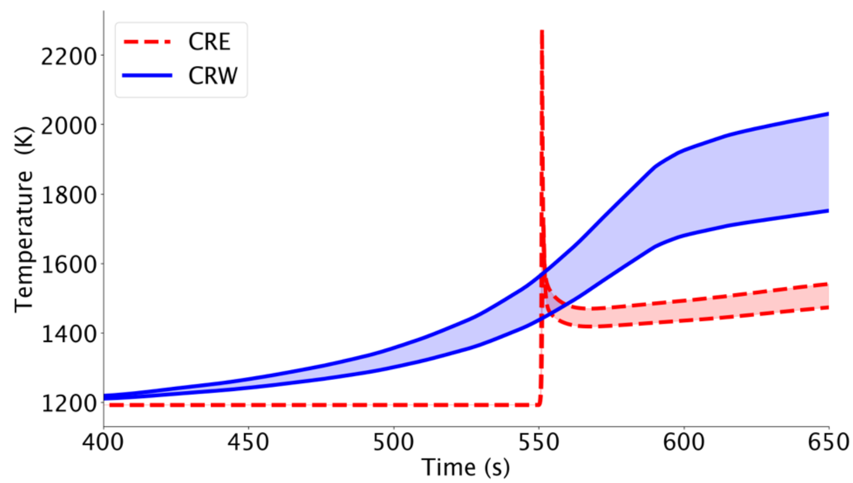

Figure 7: Fuel kernel maximum temperature range obtained for the CRW and CRE envelopes obtained with BISON.

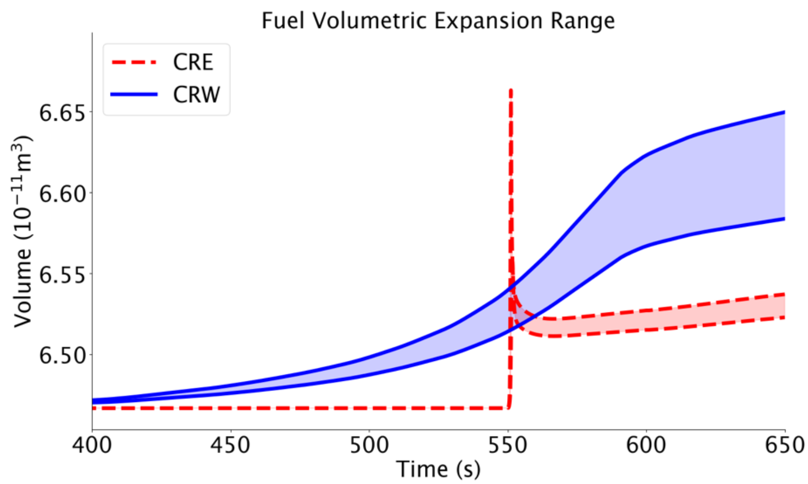

Figure 8: Fuel kernel volumetric expansion range obtained for the CRW and CRE envelopes obtained with BISON.

Table V lists maximum peak fuel temperature and energy deposition values obtained with BISON and RELAP respectively. As underlined previously for the CRW cases, the differences between the two models might be driving relative overestimations of the two considered quantities by BISON with respect to RELAP. While energy deposition results are found to be in reasonable agreement, maximum fuel temperature values differ by approximately 600 K. The reason for such a remarkable disparity is due to a contrast between the two temperature trends predicted by RELAP and BISON. While the first code predicts a quasi-monotonal increase of fuel temperature, reaching its maximum value at the end of the transient, the second tool provides a pulse-like temperature trend, as shown in Figure 7, where the peak value is attained within the duration of the transient. It needs to be underlined that the asymptotic maximum temperature value predicted by the BISON model is around 1642 K, which is in fair agreement with RELAP results if the radial thermal gradient contribution mentioned previously is considered. It is also important to remark that, as explained in detail in Ref. [7], the nature of the thermal behavior found with RELAP simulations is of a sharp temperature increase to a peak value, followed by a decrease and by a subsequent reincrease towards an asymptotic value. While the final maximum temperature values, as just mentioned, are in good agreement between RELAP and BISON, the temperature peak predicted by the RELAP model during the transient does not exceed the asymptotic temperature value as the one provided by BISON does. Overall, the two temperature behaviors are characterized by a similar nature, despite offsets in magnitude which might be led to by a number of factors that can be principally linked to the already mentioned different approximations that characterize the two models. One of the aspects that might have an influence on difference in the peaks magnitude, as underlined in the previous section, is the fact that RELAP results are given in terms of a homogenized fuel temperature, while BISON outputs refer exclusively to the center of the kernel local maximum temperature. Such a discrepancy is negligible for cases or time intervals in which the fuel kernel is close to being always in thermal equilibrium with its surroundings, while it becomes dominant if the timescale of the power variation the fuel is subject to does not allow for re-equilibration in terms of temperature between the fuel kernel and the other elements of the system. This motivation supports the fact that this type of incongruity is not observed for the CRW case, which develops at a much lower speed compared to the CRE.

Table V: RELAP and BISON maximum temperature and energy predictions.

Output variable	RELAP	BISON
Maximum energy deposition CRW (J/g)	142	146
Maximum fuel temperature CRE (K)	1619	2273
Maximum fuel temperature CRW (K)	1619	2273
Maximum energy deposition CRE (J/g)	142	146

The obtained extremes of the envelope for SiC failure probability were 1 % and 40.5 % for the minimum and maximum results respectively. It is necessary to point out once more that these results are relative to a particular input adoption that represents a worst-case scenario for what concerns the SiC layer and its failure resistance properties expressed through Weibull parameters.

The analysis of the results from the envelopes for CRW and CRE were followed by a systematic comparison between a selection of parameters that are listed in Table VI. As a first observation, the CRW scenarios are characterized by overall higher values of energy deposition and strain, both for fuel kernel and SiC, compared to the CRE. The maximum fuel temperatures for the two envelopes differ by less than 100 K, which can be reasonably considered as an insignificant offset for what concerns SiC stress state and potential failure, especially since the considered thermal regime is not characteristic of any failure-inducing phenomenon such as fuel phase transition. Despite the comparable temperature state and the generally lower energy deposition values and volumetric strains, the SiC maximum failure probability predictions for the CRE envelope were double compared to the CRW cases.

Table VI: Comparison between envelope maximum output variables for CRW and CRE.

Variable	CRW	CRE
Maximum energy deposition (J/g)	387	146
Maximum fuel temperature (K)	2180	2273
Maximum kernel volumetric strain (%)	3.5	1.35
Maximum SiC volumetric strain (%)	1.5	0.5
Maximum SiC failure probability (%)	12.88	40.5

A variety of reasons could be hypothetically driving the distinction in failure behaviors. It is necessary to underline that the analyzed results have been selected from simulations that are characterized by Weibull statistics parameters and mechanical properties that were kept consistent in the entire analysis and therefore such parameters cannot be linked to the observed difference. One of the main discrepancies, as affirmed in previous sections, between the CRW and CRE is the speed at which these transients develop. While the CRW occurs on a time span of over 200 s, the CRE develops in about 1 s or less, which is an impactful feature when considering strain rates for the materials in the system, in particular for SiC. Even though the maximum strain found with BISON is considerably higher for the CRW compared to the CRE, the latter envelope presents a maximum SiC strain rate that is more than two orders of magnitude higher than the former. Such a difference can be observed in Figure 9 and Figure 10, which present the strain envelopes for CRW and CRE respectively. It could be thus deduced that failure strain, indicated as ε_f and strain rate, indicated as $\dot{\varepsilon}$, are related as follows:

$$\varepsilon_f \propto \dot{\varepsilon}^{-1} \tag{6}$$

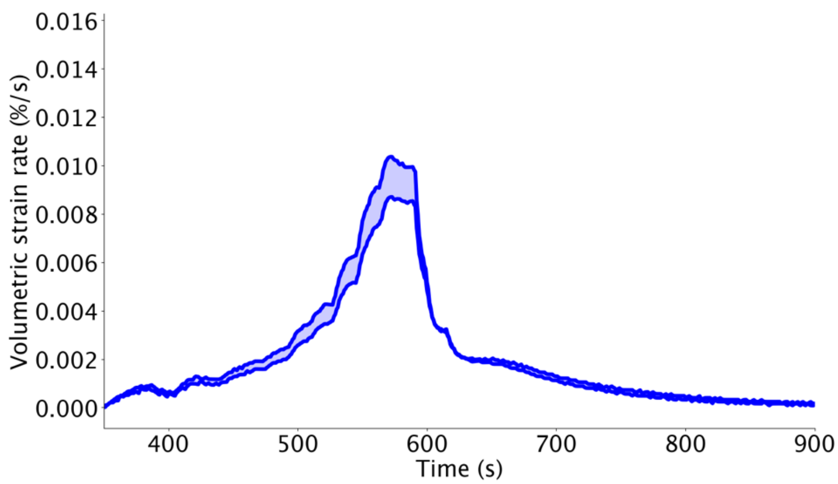

Figure 9: SiC volumetric strain rate range obtained for the CRW envelope.

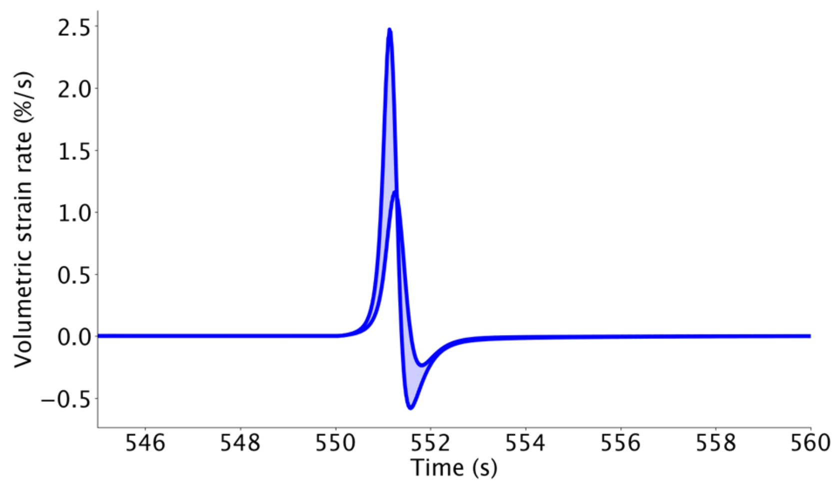

Figure 10: SiC volumetric strain rate range obtained for the CRE envelope.

Experimental evidence of an inverse proportionality relationship between failure strain and strain rate for SiC and more in general for ceramic materials can be found in literature [37-39]. The main interpretation of the role of strain rate during loading of the specimens is provided in terms of an inertia-related threshold mechanism. From an experimental perspective, the relationship expressed in Equation 6 has been hypothesized by Lankford et al. [39] to be valid only above a critical strain rate value identified as 100 s^{-1} , although Cinbiz et al. [37] have found this type of correlation to be possibly applicable at much lower strain rate values, approximately between 0.48 and 5 s^{-1}, which are closer to the strain rate regime that characterizes the scenarios analyzed in this work. It needs to be emphasized that the just mentioned studied were conducted at room temperature, while this analysis focuses on simulated thermal conditions which were between 1200 and 2200 K. A series of mechanical tests performed on SiC in a study by Samant et al. [38] with three different strain rates and at various temperatures showed a combined role of high strain rates and high temperatures in decreasing the failure strain of the specimens. Additional experimental data on SiC failure strain and strain rates relationship would be beneficial to better benchmark BISON simulation predictions and understand whether other features, such as specimen geometry and irradiation, might play a driving role in this type of mechanism.

IV.B Discussion on the conservatism of the envelopes

The boundary conditions adopted for this study were drawn from the envelopes obtained in the sensitivity study conducted in Reference [7]. Such cases were obtained, as described in previous sections, with RAVEN [9] and RELAP [2] using Sobol variance decomposition method and by sampling input parameters that were assumed to follow uniform distributions over their pre-determined domains. Convergence criteria for the study in Ref. [7] were concerned with Sobol indices and not with the values calculated by RELAP itself. During the present study, it was necessary to determine if the envelopes in Ref. [7] appropriately captured the behavior of the system during CRW and CRE events. To that end, the same parameter space was re-sampled using Latin hypercube sampling with RAVEN's stratified sampler, and the results from 10,000 cases were compared against the values obtained in Ref. [7] Potential differences could be considered important if they were to largely affect SiC failure probability predictions with respect to the results reported in sections 4.1 and 4.2. Thus, the CRW and CRE envelopes obtained by changing sampling technique could be considered consistent with those reported in Ref. [7] if no significant changes were to be found in the upper energy deposition and power limits of the envelopes, which are the conditions leading to highest SiC failure probability.

To assess whether the Latin hypercube sampling had captured the input space well, a convergence study was done varying the number of cases from as few as 1,000 to as many as 20,000. The RAVEN confidence intervals were calculated based on the percentiles of the results and do not assume any distribution of the outputs. Various increases in the number of samples were performed in order to ensure convergence of the obtained values and the results presented in this section are relative to 10,000 samples for both CRW and CRE envelopes.

Figure 11 shows the energy deposition distribution for the CRW, which presents a tail that extends to about 350 J/g. This value is below maximum deposited energy predictions by BISON but is slightly higher than the maximum energy deposition obtained by Gorton and Brown, which is 331 J/g [7]. Nonetheless, this discrepancy is not expected to have any major effects on SiC failure probability since a 20 J/g difference is not anticipated to cause an appreciable increase in tensile stresses for this type of scenario. Moreover, a relatively limited number of cases is characterized by energy depositions above 330 J/g, as it can be drawn determining the 95%-confidence intervals for the CRW energy deposition distribution. Figure 12 and Figure 13 present the 95%-confidence intervals obtained with RAVEN for energy deposition and power, respectively. The upper bound on the 95%-

confidence interval for the CRW, based on RAVEN outputs, is 321 J/g, so the maximum obtained by Gorton and Brown lies between the upper bound of the 95%-confidence interval and the maximum value obtained with Latin hypercube sampling. The mean value of energy deposition calculated by Gorton and Brown was 267 J/g, with a standard deviation of 27 J/g [7], and the mean value from 10,000 cases with Latin hypercube sampling is 267 J/g, with a standard deviation of 27 J/g. Based on the similarity in mean values, standard deviations, and maximum values, we conclude that the envelope developed in Ref. [7] is representative of the CRW, and the differences in the tails of energy deposition are not expected to yield meaningful changes in failure probability.

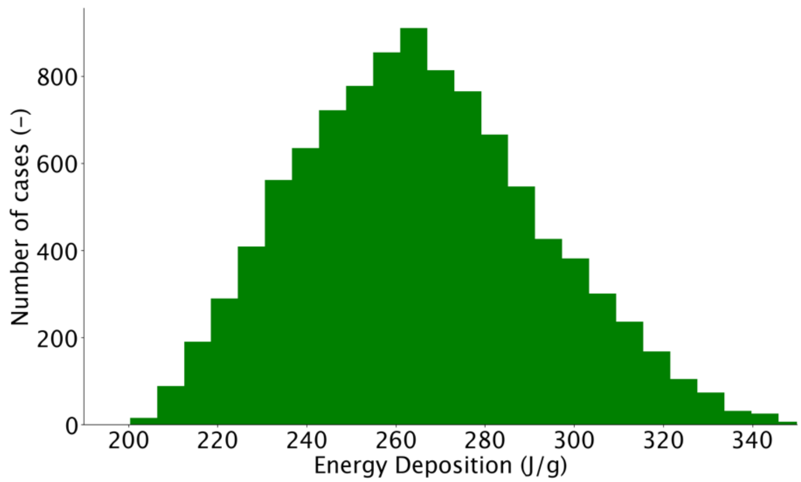

Figure 11: Energy deposition distribution for 10000 CRW cases obtained using RELAP and RAVEN's stratified sampler.

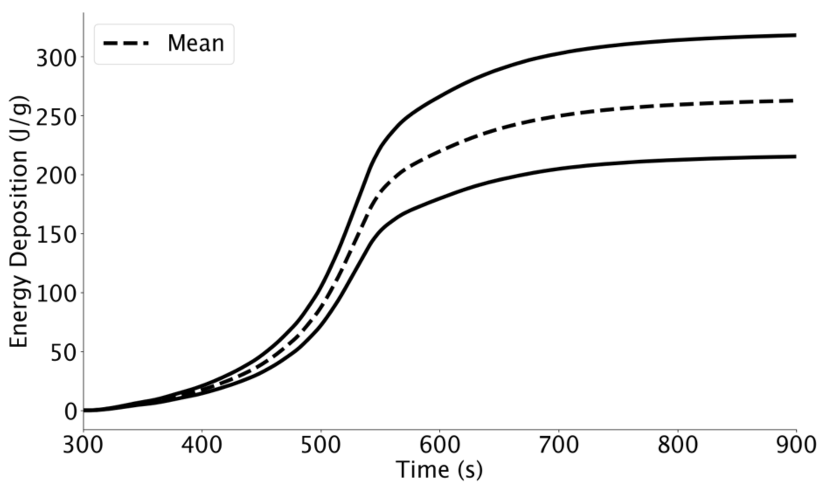

Figure 12: Energy deposition 95%-confidence interval for 10000 CRW cases obtained using RELAP and RAVEN's stratified sampler.

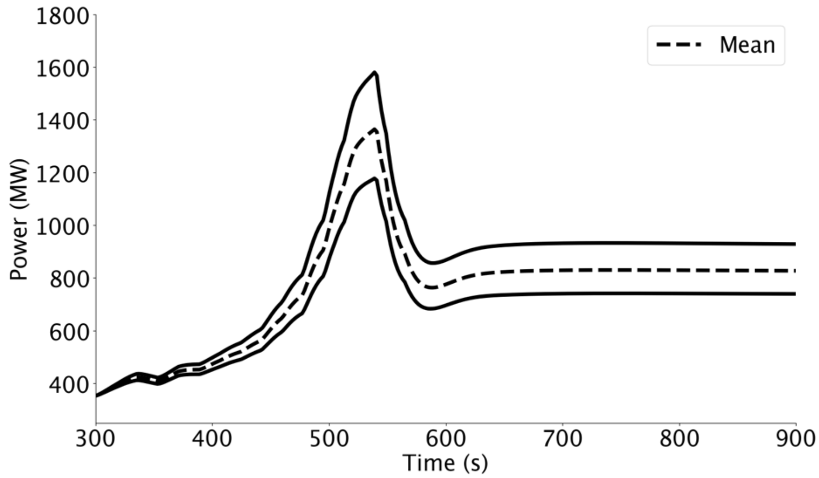

Figure 13: Power 95%-confidence interval for 10000 CRW cases obtained using RELAP with RAVEN's stratified sampler.

Figure 14 shows the energy deposition distribution for the CRE, while Figure 15 and Figure 16 depict the 95%-confidence intervals obtained with RAVEN. From Figure 14 it can be observed that the highest deposited energies are around 150 J/g. This value can be considered consistent with that obtained by Gorton and Brown [7] and with the one predicted by BISON in this analysis, which are 141 J/g and 146 J/g respectively. In fact, a variation of 10 J/g is not expected to increase SiC failure probability to values above 46%, which is the maximum value obtained in this analysis for CRE. Moreover, as similarly found for the CRW instances, the upper limit of the 95%-confidence interval extends to a value of about 140 J/g, meaning that only a limited number of cases are characterized by higher values of deposited energy. Equally to what stated for CRW, maximum power results obtained for the CRE were consistent with those found by Gorton and Brown [7], which can be further visually captured comparing Figure 16 to Figure 2. The mean value of energy deposition in CRE as calculated by Gorton and Brown is 118 J/g with a standard deviation of 12 J/g [7], and the mean value from 10,000 cases with Latin hypercube sampling is 118 J/g with a standard deviation of 11 J/g. The upper bound of the 95%-confidence interval from Latin hypercube sampling is 141 J/g, and the maximum value reported by Gorton and Brown [7] is 142 J/g, confirming once again that the envelope defined previously and used to feed the BISON analysis is representative of the CRE.

It can be thus concluded that the performance envelopes produced in Ref. [7] are representative of the CRW and CRE scenarios considered for this study and that the tails of the RELAP results would not lead to significant changes with respect to failure probability.

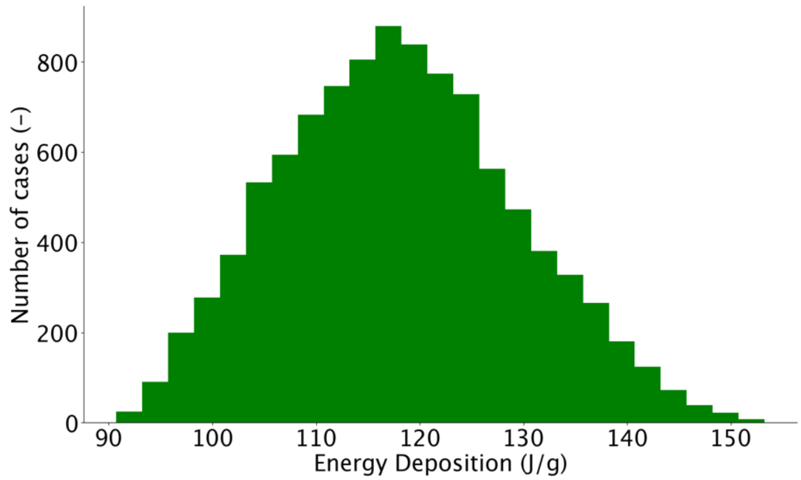

Figure 14: Energy deposition distribution for 10000 CRE cases obtained using RELAP with RAVEN's stratified sampler.

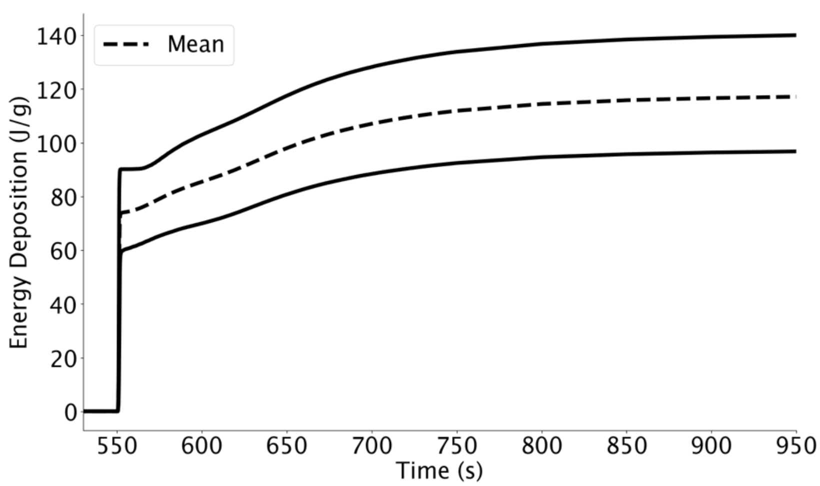

Figure 15: Energy deposition 95%-confidence interval for 10000 CRE cases obtained using RELAP and RAVEN's stratified sampler.

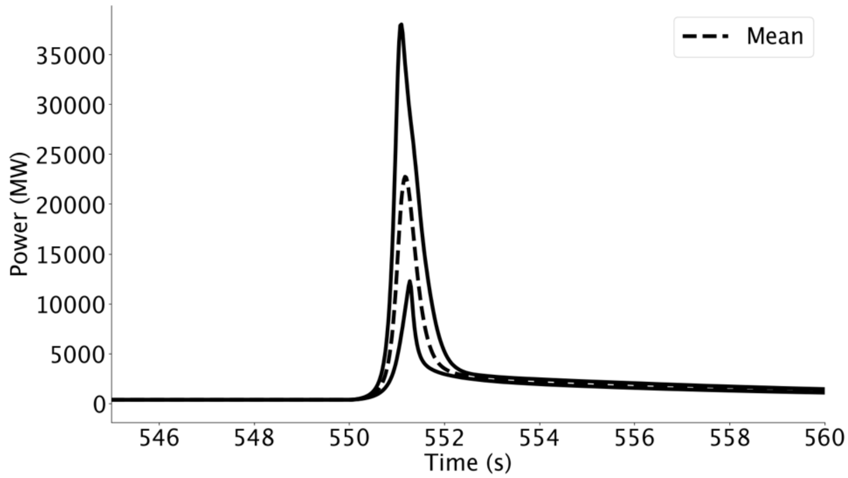

Figure 16: Power 95%-confidence interval for 10000 CRE cases obtained using RELAP and RAVEN's stratified sampler.

IV.C Sensitivity analysis

The highest and lowest SiC failure probability cases of both CRW and CRE envelopes were subject to a sensitivity analysis using the global Sobol decomposition method described in previous sections. Therefore, four cases were analyzed in total. The obtained first order and total effect Sobol indices for all involved parameters are reported in Table VII and Table *VIII*, where "high" and "low" refer to the envelope cases with maximum and minimum failure probability, respectively.

Table VII: First order effect Sobol indices for the CRW and CRE envelope extremes.

Parameter / Case	m	σ_0	V_C	r_{SiC}	ρ_{SiC}	$T_{SF,SiC}$
CRW - high	0.147	0.103	0.005	0	0	0.015
CRW - low	0.156	0.108	0.004	0	0	0.01
CRE - high	0.036	0.090	0.001	0.005	0.001	0.002
CRE - low	0.044	0.001	0	0	0	0

Table VIII: Total effect Sobol indices for the CRW and CRE envelope extremes.

Case \ Parameter	m	σ_0	V_C	r_{SiC}	ρ_{SiC}	$T_{SF,SiC}$
CRW - high	0.816	0.791	0.009	0.01	0	0.115
CRW - low	0.823	0.773	0.093	0.016	0	0.078
CRE - high	0.557	0.817	0.092	0.047	0	0.067
CRE - low	0.141	0.216	0.036	0.025	0.03	0.13

A convergence study involving several sample sizes, ranging from 1400 to 42000, was conducted in order to assess stable Sobol indices. Convergence was determined qualitatively based on the reduction of oscillations in first order effect and total effect Sobol index values as sample size was increased. For all analyzed cases, stabilization of Sobol indices was obtained for sample sizes of 28000. The results reported hereafter refer to samples sizes equal to 42000. Figure 17 and Figure 18 show total effect and first order effect Sobol indices for the upper CRW envelope and lower CRE envelope extremes, respectively, as a function of sample size. It can be visually inferred how in both cases index variation is strongly reduced for all input parameters for sample sizes above 28000.

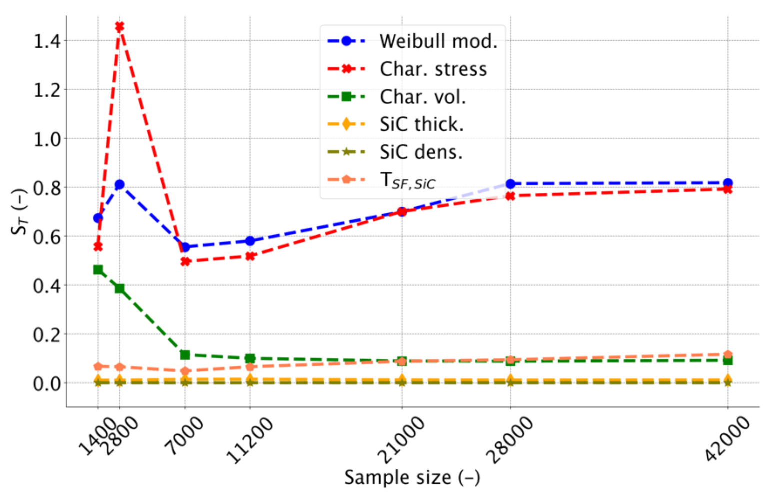

Figure 17: Total effect Sobol indices as a function of sample size for the highest-failure-probability CRW envelope case.

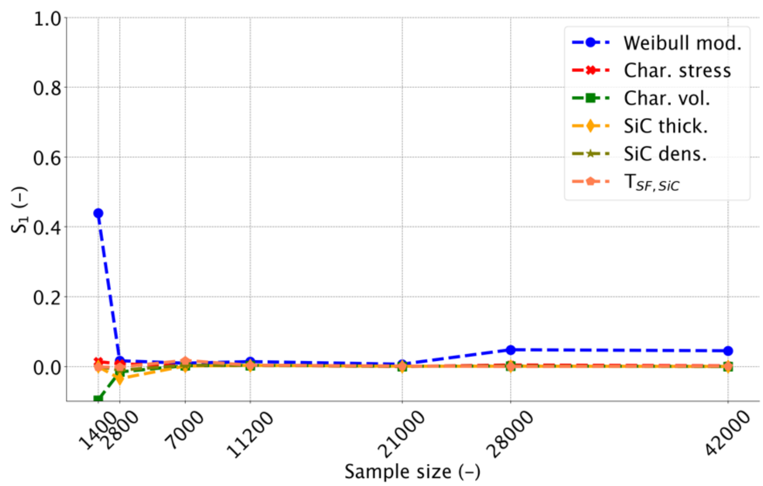

Figure 18: First order effect Sobol indices as a function of sample size for the lowest-failure-probability CRE envelope case.

Figures 19 through 22 show the first order effect and total effect Sobol indices for all the analyzed scenarios and it can be observed that the most important parameters with respect to SiC failure probability are Weibull modulus and characteristic stress. While Figure 19, 20 and 21 show that the influence of such inputs is evident, Figure 22, which corresponds to the lowest failure probability scenario for the CRE envelope, does not illustrate such a remarkable impact. Figure 19 and Figure 20 refer to the highest and lowest failure probability cases for the CRW envelope and in both cases m is the most impactful input, while σ_0 is characterized by close, though slightly lower, S_1 and S_T values for such scenarios. Figure 21 and Figure 22 are linked to the highest and lowest failure probability cases for the CRE envelope and for these scenarios the most important parameter is characteristic stress, followed by the Weibull modulus. As stated previously, two differences can be pointed out between CRW and CRE scenarios and they can be expressed in terms of:

1) Energy deposition: CRW instances are characterized by higher deposited energy values with respect to CRE ones and there is a direct proportionality between energy deposition and SiC failure probability, as found also in previous studies [5]. Specifically, if we refer to the analyzed cases, Figure 19 and Figure 22 refer to the highest and lowest energy deposition scenarios, respectively.
2) Strain rate: as discussed in section 4.3, CRE cases are faster transients and are characterized by higher strain rates compared to CRW scenarios.

Following the preceding points, firstly it can be stated that the Sobol index magnitude, and thus the impact of the involved input parameters on SiC failure probability predictions, is dependent on the energy deposition regime. This feature can be better understood observing Figure 21 and Figure 22: the two cases, with respect to the entirety of this analysis, are in a low deposited energy regime, for which Sobol indices appear to be proportional to energy deposition. The same does not apply to CRW cases, which are characterized by a higher deposited energy interval for which the lower bound is distinctively higher than the upper CRE energy deposition limit. Secondly, slower transients (Figure 19 and Figure 20) appear to be characterized by m having a stronger effect than σ_0 on SiC failure probability, while the opposite happens for faster transients (Figure 21 and Figure 22). It can be stated that the relative predominance of either Weibull modulus or characteristic stress on influencing SiC failure probability depends on the speed at which the transient develops and thus on the strain rate. Additional studies of this type on a wider spectrum of energy depositions and strain rates would be beneficial to better understand these dependencies. Nonetheless, these findings are of particular interest for future analyses since BISON SiC failure probability predictions are not expected to depend on Weibull parameters sets unequivocally. From this analysis it emerges that the strain rate and energy deposition regime need to be considered as they are anticipated to influence the impact of both m and σ_0.

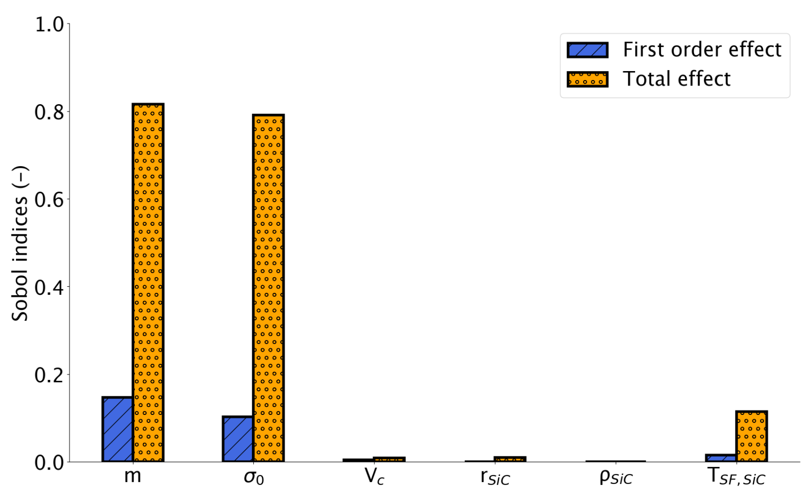

Figure 19: Sobol indices for the highest-failure-probability case of the CRW envelope.

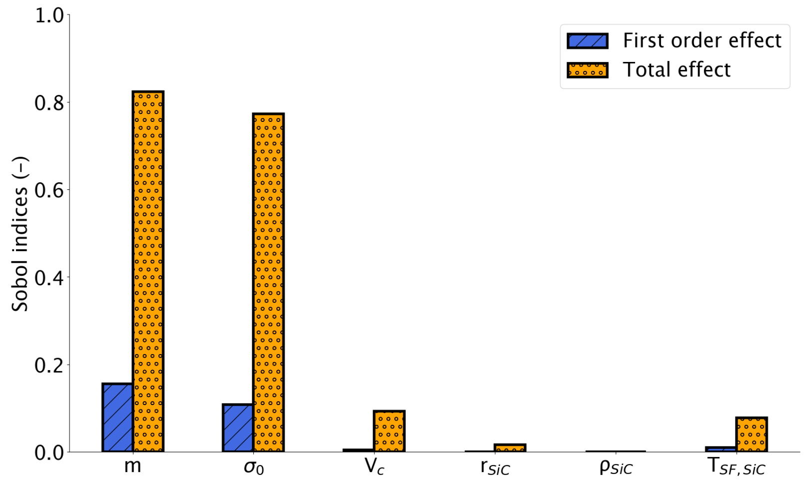

Figure 20: Sobol indices for the lowest-failure-probability case of the CRW envelope.

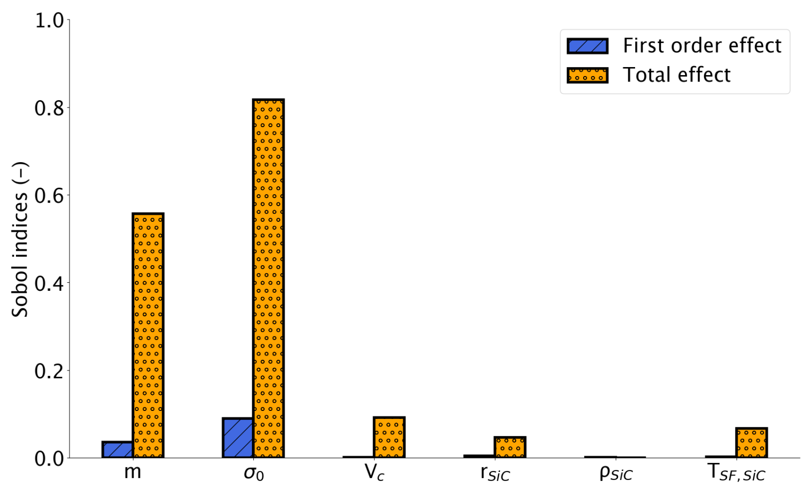

Figure 21: Sobol indices for the highest-failure-probability case of the CRE envelope.

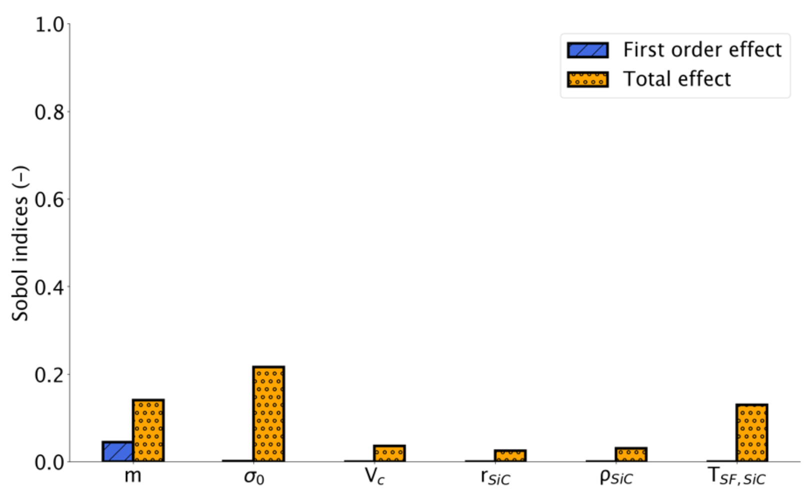

Figure 22: Sobol indices for the lowest-failure-probability case of the CRE envelope.

IV.D SiC failure probability confidence intervals

The failure probability predictions for SiC in worst case conditions for both CRW and CRE reported in Section IV.A were computed, as previously mentioned, using the Weibull parameters set shown in Table III, which is characteristic of a rather weak SiC TRISO layer [8]. Subsequently, an approach proposed in a previous study [8] and based on utilizing intervals of Weibull parameters rather than fixed sets was considered. To obtain the quantitative degree of variability around failure probability predictions, confidence intervals were computed by propagating the uncertainties around Weibull modulus, characteristic stress and characteristic volume. In addition to the set presented in Table III, three supplementary Weibull parameters sets were considered for the analysis. The sets of parameters were retrieved from available data on hemispherical SiC shells [23]. All three parameters sets were assumed as normally distributed with standard deviations equal to selected uncertainties available in the literature [18, 40, 41]. The standard deviation associated to characteristic stress was set to 50 MPa assuming it equal to the available uncertainty values around SiC fractures stress measurements [41]. The Weibull modulus standard deviation, on the other hand, was set qual to 1 following expected uncertainties from statistical evaluation of estimators for this variable [40]. The standard deviation related to the characteristic volume was derived from statistical variations regarding TRISO dimensions [18]. Table *IX* displays the mean and standard deviation values for all involved sets of parameters, indicated with μ_i and σ_i respectively for each parameter i, which were adopted to sample inputs via Python using SALib [30]. Going from set A to set D, the adopted inputs were expected to induce progressively lower SiC failure probability values for the examined conditions as they are representative of increasingly stronger SiC layers. BISON input files were subsequently run for the maximum failure probability case of each involved envelope. SiC failure probability output distributions were successively post-processed to extract confidence intervals. Specifically, such data were fitted to beta distributions since normal distribution fitting was not possible due to the relative asymmetry of the obtained outputs. Initially, three sample sizes were used to assess whether confidence intervals results would depend on the number of samples for the involved parameters. In particular, sample sizes equal to 800, 4000 and 12000 were utilized and since no appreciable difference was found between the second and third sample dimensions, no further increase was carried out. The results presented in this section are relative to sample sizes equal to 12000.

Table IX: Input distribution features used confidence intervals computation [18, 40, 41].

Set	μ_m (-)	σ_m (-)	μ_{σ_0} (MPa)	σ_{σ_0} (MPa)	μ_{V_C} (10^{-10} m^3)	σ_{V_C} (10^{-10} m^3)
A	3	1	350	50	1.5	0.5
B	4.3	1	550	50	1.5	0.5
C	7.45	1	1100	50	1.5	0.5
D	7.45	1	1808	50	1.5	0.5

Figure 23 and Figure 24 show the output failure probability distributions for the considered CRW and CRE cases simulated using the Weibull parameters set A. All the analyzed distributions have been fitted to beta distributions and the relative 95%-confidence intervals are listed in Table X and Table *XI*. Figure 25 and Figure 26 depict the trend of failure probability confidence intervals width as a function of the selected parameters set. It can be drawn how, going from set A to set D, the confidence interval widths strongly reduce to values that closely approach zero. It can thus be affirmed that sets C and D represent accident-bearing SiC TRISO layers from a Weibull-parameters perspective, while sets A and B cannot be considered good candidates to be subject to type of conditions examined in this work.

From Figure 25 and Figure 26 it can be observed that the width of the confidence intervals obtained with set A is rather large with respect to those obtained with the other sets. The reason for such discrepancy is found when considering the relative impact of the variation of Weibull modulus and characteristic stress on SiC failure probability, as underlined in section 4.5 through the obtained Sobol sensitivity indices. Although the performed variation of such parameters for this analysis is within their experimental uncertainties around nominal values, even small perturbations in m or σ_0 can induce substantial deviations in SiC failure probability outputs. The quantitative impact that a variation of Weibull parameters can have on failure probability can be better captured examining Figure 27, which shows SiC failure probability as a function of characteristic stress for a scenario where the value of m and V_C are 3 and $1.5 \cdot 10^{-11}$ m^3 respectively and tensile stresses are assumed to be uniaxial and equal to 300 MPa. The ellipsoidal shape in Figure 27 underlines how by varying the value of σ_0 between 250 and 350 MPa a rapid change in failure probability is found. In particular, as characteristic stress increases of around 100 MPa, SiC failure probability decreases from about 80 % to 20 %, which supports the findings presented in Table X and Table *XI*. Moreover, the additional uncertainties around both Weibull modulus and characteristic volume further contribute to widen the interval of SiC failure probability BISON predictions. It needs to be underlined that the observed degree of variability is not to be expected for higher characteristic stress values that are located further with respect to the previously emphasized inflection area in Figure 27. If a σ_0 variation of about $\pm$ 50 MPa around 500 MPa is considered, Figure 27 shows that a failure probability variation is obtained of approximately 10 %, meaning that input uncertainties are less impactful if considered for stronger SiC TRISO layers. The results presented in this section are a valuable contribution to current literature as they underline how, for weak SiC TRISO layers, even an infinitesimal degradation in mechanical properties can lead to strong variations in failure behavior. Likewise, this study demonstrates that an accurate BISON TRISO failure analysis cannot prescind from producing a failure probability distribution based on Weibull parameters sets, along with their relative uncertainties, since the exclusion of any type of uncertainty range would not allow for determining the possibly high degree of variation of SiC failure probability around nominal values. Moreover, this type of analysis can serve as a powerful tool to inform future industrial quality control on TRISO particles in terms of SiC layer properties. As previously stated in this section, sets A and B were associated to SiC failure probabilities confidence intervals which encompassed values that would not render the respective SiC layers able to withstand the scenarios analyzed in this work. On the other hand, sets C and D are representative of stronger SiC layers that would be able to tolerate the considered accident conditions. The categorization of SiC layers between either acceptable or non-acceptable, from a thermomechanical perspective, necessitates to include investigations in terms of the associated Weibull parameters.

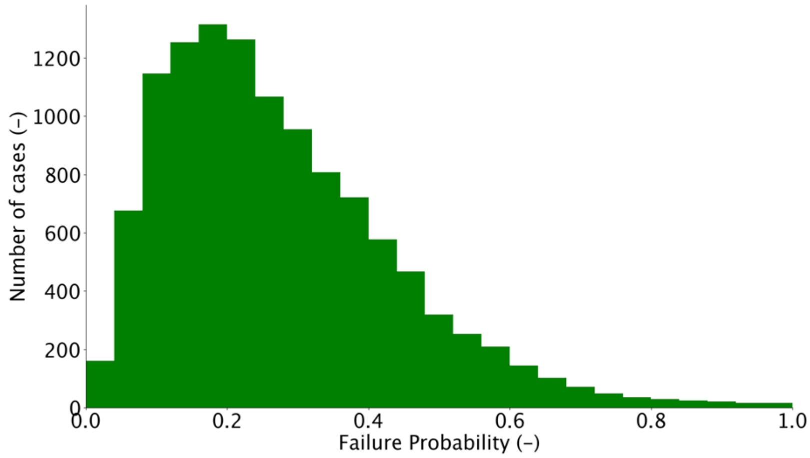

Figure 23: SiC failure probability output distribution for the upper CRW envelope extreme obtained with Weibull parameters set i.

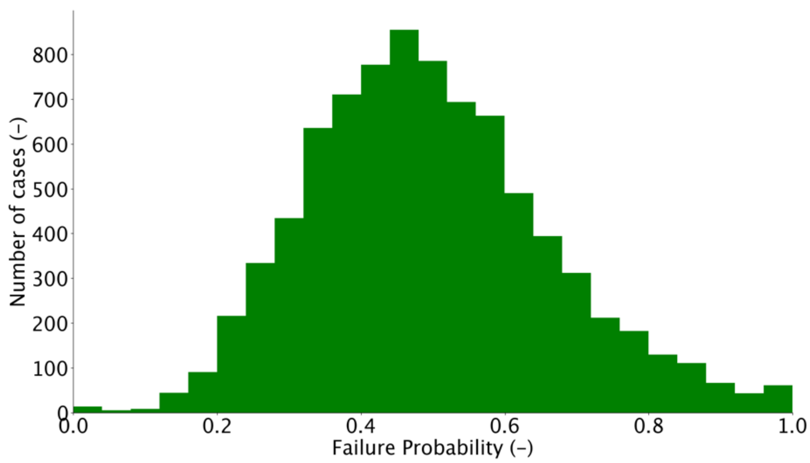

Figure 24: SiC Failure probability output distribution for the upper CRE envelope extreme obtained with Weibull parameters set i.

Table X: 95% confidence interval bounds for the CRW failure probability envelope upper extreme.

Set	**Lower bound (%)**	**Upper bound (%)**
A	1.97	49.63
B	0.02	7.52
C	$6.96 \cdot 10^{-6}$	$1.08 \cdot 10^{-3}$
D	$3.35 \cdot 10^{-9}$	$1.05 \cdot 10^{-4}$

Table XI: 95% confidence interval bounds for the CRE failure probability envelope upper extreme.

Set	**Lower bound (%)**	**Upper bound (%)**
A	14.6	85.2
B	0.7	24.2
C	$6.65 \cdot 10^{-3}$	0.03
D	$3.75 \cdot 10^{-6}$	$7.96 \cdot 10^{-4}$

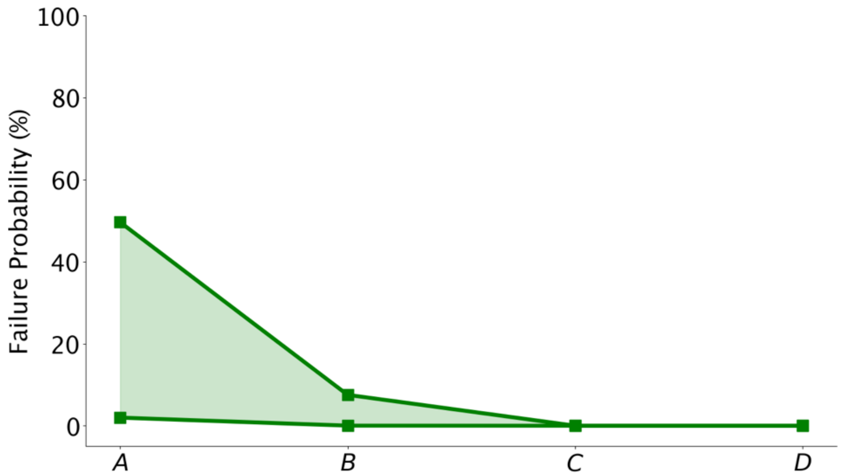

Figure 25: 95 % confidence intervals width as a function of the selected Weibull parameters set for the CRW envelope upper extreme.

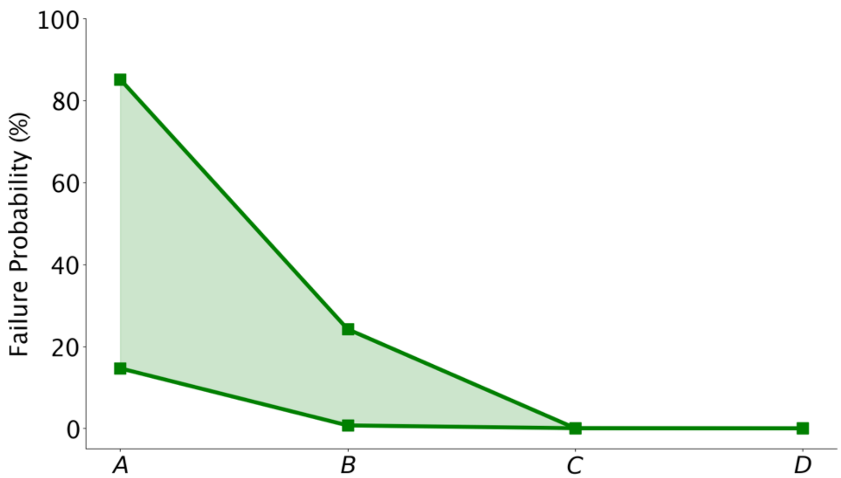

Figure 26: 95 % confidence intervals width as a function of the selected Weibull parameters set for the CRE envelope upper extreme.

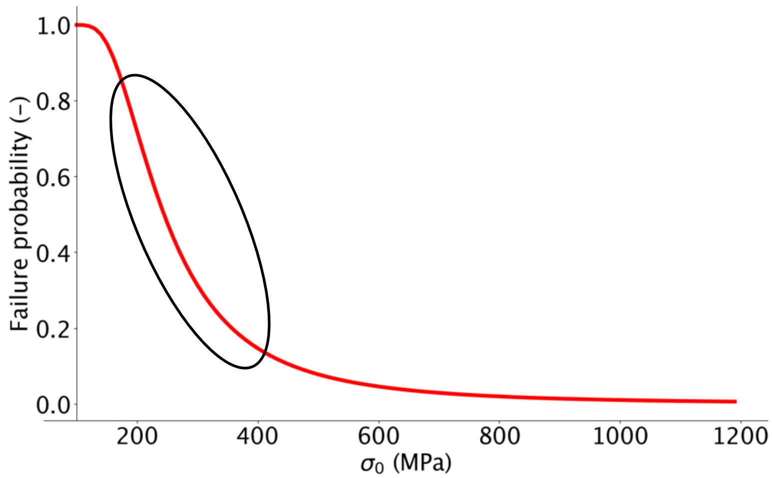

Figure 27: SiC failure probability as a function of characteristic stress for an applied external tensile stress of about 300 MPa and Weibull modulus equal to 3.

IV.E Categorization approach of SiC TRISO layers for quality control applications

The 95%-confidence intervals presented in section 4.6 were obtained using, as mean for the normal distributions, Weibull modulus and characteristic stress values associated to hemispherical SiC specimens. Such data were obtained in a study by Hunn et al. [23] that determined the Weibull parameters sets associated with multiple batches of chemical vapor deposited SiC shells via a modified crush testing technique, for which an in-depth description of experimental setting and procedure can be found in Ref. [23]. The evidence presented in section 4.6, particularly regarding sets A and B, for which SiC failure probability reached considerable values during the transient, demonstrates the need for determining a SiC classification criterion based on Weibull parameters. Such a categorization also satisfies what emphasized in the "Proposed Adaptation of the Standard Review Plan NUREG-0800, Chapter 4 (Reactor) for Sodium-Cooled Fast Reactors and Modular High-Temperature Gas-Cooled Reactors" [42]:

"To meet the requirements of 10 CFR 50, Appendix B, a statistically-based Fuel-Production Quality Assurance Plan (FPQAP) must be established that addresses all quality requirements for the fabrication of the fuel system. […] The as-manufactured fuel quality criteria shall assure manufacturing and quality control processes are in place for the coated particle fuel that results in; (1) a robust TRISO-coated fuel particle that will experience a low fraction of

incremental particle failure during normal operation, including AOOs, and DBEs/DBAs, with a high statistical certainty, and (2) a very small beginning-of-life (BOL) defective particle fraction as evidenced by the level of heavy metal (HM) contamination and defect particle fraction levels. […] To assure an acceptable product, specific properties for each fuel component, defined quantitatively in a Fuel Product Specification, are sampled using statistically accepted methods, measured using standardized procedures, and the results statistically analyzed. Acceptance can be based on the property value as well as its statistical certainty compared to the specification. In this manner the manufacturing processes can be proven to meet specifications with high statistical confidence. This method of statistical process control applies to the production of all fuel components including: […] TRISO coating – Properties controlled for each of the four layers of the TRISO coatings applied to fuel kernels are: dimensions (thickness of each layer and particle aspect ratio); density of each layer; microporosity of iPyC and oPyC layers; anisotropy of the iPyC and oPyC; defective coating fractions ((a) missing or defective buffer layers; (b) missing or defective iPyC layers; and (c) missing or defective oPyC layers); and in particular for the SiC coating: density, crystallographic phase, grain size and orientation, and Weibull properties (characteristic strength and modulus).”

The intended classification of SiC layers based on Weibull material properties constitutes a solid tool to inform future Fuel-Production Quality Assurance Plans (FPQAP) involving TRISO fuel, since it provides both a fuel-performance-based estimate of SiC failure probability and its relative uncertainty, built upon 95%-confidence intervals, for each established quality category. Given the considered accident instances, the analysis performed in previous sections showed that the most challenging conditions that the fuel might experience are related to the CRE scenario, which is thus conservative with respect to CRW from a SiC failure probability perspective. If the results in Table XI are considered, it can be observed that sets A and B are not to be defined acceptable for reactor operation due to the associated:

i) SiC failure probability regimes: both set A and set B are characterized by failure probability intervals whose upper bounds are above 80 % and 20 % respectively.

ii) SiC failure probability uncertainty: the 95%-confidence intervals widths for both sets exceed multiples of ten percent, which compromises statistical accuracy for the associated failure probability estimates.

On the other hand, sets C and D, as stated in section 4.6, could be considered acceptable both from a SiC failure probability regime perspective and from an uncertainty standpoint. If, for instance, the 95 %-confidence interval upper bound for set D, shown in Table XI, was to be extended to a TRISO population equal to a million, eight particles at most would be found to fail under CRE accident conditions. Based on the obtained results for the two sets, it can be affirmed that two necessary conditions are to be satisfied in order to obtain SiC failure probability values that are within the ranges listed in Table X and Table XI for the CRW and CRE respectively for sets C and D. Table XII lists two proposed sets of necessary conditions for Weibull modulus and Characteristic stress, along with the associated maximum number of failed particles, N_f, under CRE conditions for a population of 10^6 particles. The motivation behind the inclusion of both a condition on Weibull modulus and one on characteristic stress lies in the necessity to ensure that the associated failure probability estimates along with their related uncertainties, whose order of magnitude can be estimated through the width of the 95%-confidence intervals, are acceptably low. Depending on the perimeter of application of the involved TRISO particles, the degree of acceptability for SiC failure probability values and the associated uncertainties can be relatively stringent. In this analysis, SiC failure probability values and uncertainties above 1 % were assumed as an upper bound for adequacy of the relative Weibull parameters ranges. An argument could be proposed in favor of using other types of necessary conditions on either Weibull modulus or characteristic stress to categorize SiC TRISO layers. In particular, SiC layers characterized by relatively low values of Weibull modulus, or characteristic stress, could be proposed to be acceptable if they were accompanied by relatively high characteristic stresses or Weibull moduli, respectively. Such an option cannot be considered suitable because, when varying Weibull modulus or characteristic stress within their pre-determined uncertainty ranges in low-value regimes, a rather large variation in SiC failure probability will be found as a result, as it has been also underlined with Figure 27. To quantitatively exemplify the importance of the variation of Weibull parameters within low-value domains, four simulations were run for the CRW scenario with Weibull parameters sets that are listed in Table *XIII*, along with the resulting SiC failure probability predictions from BISON. The first two rows of Table *XIII* differ in terms of characteristic stress, which has been varied according to its experimental uncertainty, as shown in Table IX. Likewise, the third and fourth rows of Table *XIII* show two parameters sets used to perform BISON CRW simulations with Weibull modulus values that were changed following experimental uncertainties listed in Table IX. It can be understood from the associated SiC failure probability results how variations of either m or σ_0 within their uncertainties in low-value regimes induce SiC failure probability changes of more than 3 %. Moreover, failure probability predictions extend to maximum values of around 4 %. Such results on SiC failure probability and its considerable fluctuations induced by low-value Weibull parameters uncertainties render the additional previously hypothesized conditions not suitable for determining safety limits for SiC TRISO layers. Instead, a double-condition approach, as the one provided in Table XII, is to be preferred to ensure higher SiC quality along with statistical accuracy.

Table XII: Minimum m and σ_0 necessary to obtain the associated N_f.

$\boldsymbol{Minimum\ m}\ (-)$	$\boldsymbol{Minimum\ \sigma_0}\ (\boldsymbol{MPa})$	$\boldsymbol{Maximum\ N_f}\ (-)$
7.45	1100	300
7.45	1808	8

Table XIII: Weibull parameters sets and SiC failure probability predictions for CRW for hypothetical supplementary safety conditions testing.

$\boldsymbol{m}\ (-)$	$\boldsymbol{\sigma_0}\ (\boldsymbol{MPa})$	$\boldsymbol{V_c}\ (\boldsymbol{10^{-10}\ m^3})$	$\boldsymbol{F_p}\ (\%)$
7	350	1.5	1.6
7	300	1.5	4.5
3	1100	1.5	0.7
2	1100	1.5	4

In this preliminary stage, it is necessary to consider the available options without including yet a binary framework that discriminates between acceptable and non-acceptable parameters ranges, as performed for sets A and B. While it is clearly comprehensible why sets A and B are not suitable examples of functional SiC for reactor applications, a definitive assessment of the degree of acceptability of the ranges listed in Table XII is out of the scope of this analysis. The maximum number of particles that can be allowed to fail during the considered accident scenarios is dictated by the associated radioactive source, which in turn depends on several factors, including burnup and enrichment. Consequently, the definition of a unique threshold that could serve as a benchmark for the values reported in Table XII was considered out of the framework of this study. Nonetheless, the results provided by this research supply data necessary to inform safety analyses based on mechanical testing to be integrated within the space of future FPQAPs.

To provide a practical illustrative application of the proposed double-condition categorization scheme, the data obtained by Hunn et al. [23] for hemispherical SiC shells was divided into three classes:

- Class I: SiC layer characterized by $m \geq 6$ and $\sigma_0 \geq 1000\ MPa$.
- Class II: SiC layer characterized by $3.5 \leq m < 6$ and $450\ MPa \leq \sigma_0 < 1100\ MPa$.
- Class III: SiC layer characterized by m and σ_0 values not included within the two previous classes.

Figure 28 shows the percentage of hemispherical SiC shells from Ref. [23] falling within each class. It is necessary to underline that the results shown in Figure 28 are not representative of realistic TRISO particles to be used in reactor applications. In particular, the TRISO batches utilized in Ref. [23] were characterized by a wide variety of SiC qualities. It is fundamental to state that such a degree of assortment is not going to be present within future industrially produced TRISO batches, due to rigorous quality control.

The total number of SiC specimens analyzed in Ref. [23] was equal to 567. As it can be observed from Figure 28, the percentage of specimens included in Class I, which covers the domain of the previously analyzed sets C and D, is around 10 %. The remaining 90% of specimens are encompassed by Classes II and III, which in turn incorporate the Weibull parameters regimes for sets A and B. It is fundamental to underline once again that the data categorized in Figure 28 is not representative of identical particles, since several experimental and physical features were varied in the production of the various tested batches. Characteristics such as SiC deposition temperature, thickness and other experimental settings were altered for different groups of specimens. It is equally necessary to emphasize that the classes defined above are solely based on the analysis performed in this study which is founded on the assumption of CRW and CRE being the most challenging circumstances for TRISO fuel, since the focus of this work is on the HTGRs framework. Moreover, it is crucial to emphasize once more that the resulting fractions presented in Figure 28 are not descriptive of realistic batches of identical coated particles designed for reactor operation. This part of the work is aimed demonstrating that the presented safety approach constitutes a re-appliable scheme that needs to be precisely targeted to the intended TRISO fuel application. Other types of reactors that operate with TRISO, such as Fluoride salt-cooled High-Temperature Reactors (FHRs) [43], are expected to pose conditions that are diverse and possibly less challenging to the fuel with respect to the ones explored in this study. Therefore, Weibull-parameters-based safety limits need to be adapted to the specific design of interest. Moreover, the integration of the presented fuel-performance-based safety limits with additional experimental data regarding SiC mechanical performance for both fresh and burnt TRISO fuel would be of great benefit in order to allow for a thorough and informed definition of quality classification criteria for coated fuel particles.

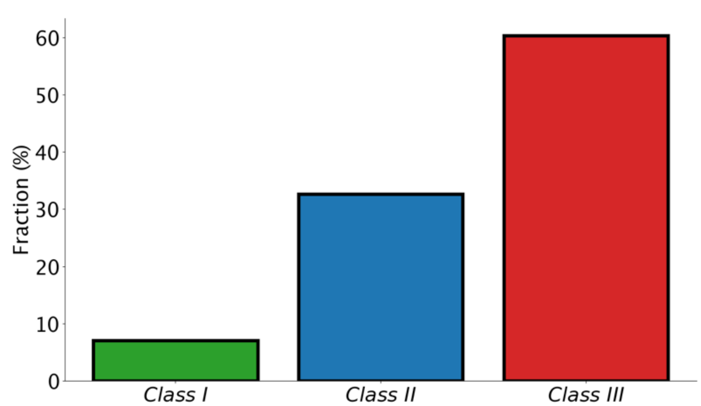

Figure 28: Fraction of hemispherical SiC shells tested in Ref. [23] belonging to each defined Weibull-parameters-based class.

V. Conclusion

This work focused on the study of the failure behavior of TRISO SiC layer during two types of HTR RIA scenarios with BISON. Boundary conditions for the analyzed cases, specifically a group Control Rod Withdrawal (CRW) and a Control Rod Ejection (CRE) were obtained by reproducing results from a previous study by Gorton and Brown [7] with RELAP and RAVEN. A single particle 1D TRISO model with a UO_2 kernel was used to simulate the provided scenarios in BISON. Performance envelopes produced in Ref. [7] for the two accidents were propagated with BISON and their exhaustiveness with respect to RELAP input space span was assessed and confirmed by the generation of new envelopes with the adoption of a different sampling technique. Specifically, envelopes produced with RELAP and RAVEN using the same input domains chosen by Gorton and Brown [7] but different sampling scheme did not yield any changes, in terms of power and energy deposition, that would, once propagated in BISON, translate into substantial variations of SiC failure probability. Consequently, the envelope produced by Gorton Brown [7] was confirmed to be representative of HTGR RIA scenarios.

One of the fundamental findings of this study is that, even though the CRW envelope BISON predictions, when compared to CRE ones, were found to be characterized by higher values for energy depositions, final fuel temperature, fuel volumetric strain and SiC volumetric strain, the range of SiC failure probability peaked at 23 %, while the CRE one extended to 46 %. This discrepancy is attributed in this work to the inherent mechanical kinetics of the simulated events, since the strain rate in the CRE envelope was about two orders of magnitude higher with respect to that found for CRW scenarios and experimental findings available in literature support an inverse proportionality relationship between failure strain and strain rates in ceramics such as silicon carbide.

Another important aspect of this work was the sensitivity analysis performed on SiC failure probability BISON predictions that involved various input variables such as Weibull parameters, as well as SiC stress-free temperature, thickness and density. Results showed that the two most important factors impacting SiC failure probability were Weibull modulus and characteristic stress and that their relative importance depended on the specific case. In particular, the variation of the impact of such variables in this analysis was identified as dependent on both energy deposition and strain rate.

An additional contribution of this work was the determination of confidence intervals for four sets of Weibull parameters. Confidence intervals were obtained by varying Weibull input parameters over uncertainty-based ranges for the highest SiC failure probability cases for both CRW and CRE. The obtained 95 % confidence intervals were relatively wide for two of the analyzed sets of parameters, and it was found that the width of the confidence intervals decreased as the values of both Weibull modulus and characteristic stress were increased. For the parameters sets characterized by wide confidence intervals, the degree of variability of SiC failure probability induced by even relatively small changes in input Weibull parameters was ascribed to the intrinsic failure behavior of weak SiC layers and it demonstrated the importance of including uncertainty ranges for input parameters when performing failure analyses of this kind in BISON. The analyzed Weibull parameters sets BISON outputs, along with the associated failure probability confidence intervals, were used to propose a new double-condition based criterion for SiC quality classification. The two conditions impose minimum values on both Weibull modulus and characteristic stress in order to ensure a maximum SiC failure probability under HTGR accident conditions. The maximum predicted SiC failure probability values do embed input Weibull parameters uncertainties, which contributes strengthening the conceived methodology. The proposed SiC categorization scheme constitutes a replicable method that provides both fuel-performance-based SiC failure probability estimates and low uncertainties which are proportional to the obtained 95%-confidence intervals widths. The specific limits for the Weibull parameters cannot be generalized since they strictly depend on the TRISO application of interest and the lower Weibull parameters bounds listed in this study are defined within the scope of HTGRs. The approach presented in this work serves as a solid basis for systematic evaluation of TRISO fuel quality from a mechanical perspective to be integrated in prospect Fuel-Production Quality Assurance Plans (FPQAPs).

Future work should focus on expanding the approach presented in this study to other accident scenarios by coupling RELAP and BISON. Particularly, extending this type of analysis to a wider variety of energy depositions and strain rates would be of great value to enhance the understanding of their impact on failure probability results. Additionally, depending on the availability of new experimentally based literature on the dependence of failure strain on strain rate, modeling efforts should be also directed towards benchmarking BISON predictions against accessible data. Moreover, prospect analysis involving SiC mechanical performance in BISON should include uncertainty ranges or Weibull parameters intervals, as performed in this analysis, and should propagate such uncertainties onto simulated SiC failure probability in order to express predictions in terms of envelopes and ranges, rather than fixed values, in order to encompass the high degree of variability of the evaluated quantity for low Weibull parameters values. Forthcoming efforts should also focus on extending the proposed approach for the definition of double-condition-based safety limits for Weibull parameters on other types of designs that operate with TRISO fuel. Such safety limits are strongly influenced by the accident scenarios perimeter which in turn is contingent on the specific application. Such motivations render an ad-hoc Weibull parameters lower bounds definition necessary for each individual reactor type.

Acknowledgments

The authors would like to acknowledge Dr. Daniel Schappel at Oak Ridge National Laboratory and Professor Brian D. Wirth at the University of Tennessee, Knoxville for the helpful discussions on BISON and TRISO.

The analyses performed in this study were performed as follows: RELAP simulations were performed by Robert F. Kile and BISON calculations were carried out by Carlotta G. Ghezzi.

This work was funded by a U.S. Department of Energy Integrated Research Project led by Prof. Wirth entitled: “Multi-physics fuel performance modeling of TRISO-bearing fuel in advanced reactor environments”.

This research made use of Idaho National Laboratory computing resources which are supported by the Office of Nuclear Energy of the U.S. Department of Energy and the Nuclear Science User Facilities under Contract No. DE-AC07-05ID14517.

References

[1] N.R. Brown, A review of in-pile fuel safety tests of TRISO fuel forms and future testing opportunities in non-HTGR applications, Journal of Nuclear Materials, 534 (2020) 152139.
[2] INL, RELAP5-3D Code Manuals, Volumes I-IV and Appendix A, INL/MIS-15-36723- V2, Idaho National Laboratory, 2015.

[3] R.L. Williamson, J.D. Hales, S.R. Novascone, G. Pastore, K.A. Gamble, B.W. Spencer, W. Jiang, S.A. Pitts, A. Casagranda, D. Schwen, A.X. Zabriskie, A. Toptan, R. Gardner, C. Matthews, W. Liu, H. Chen, BISON: A Flexible Code for Advanced Simulation of the Performance of Multiple Nuclear Fuel Forms, Nuclear Technology, 207 (2021) 954-980.
[4] M. Umeda, T. Sugiyama, F. Nagase, T. Fuketa, S. Ueta, K. Sawa, Behavior of coated fuel particle of high-temperature gas-cooled reactor under reactivity-initiated accident conditions, Journal of nuclear science and technology, 47 (2010) 991-997.
[5] D. Schappel, N.R. Brown, K.A. Terrani, Modeling reactivity insertion experiments of TRISO particles in NSRR using BISON, Journal of Nuclear Materials, 530 (2020) 151965.
[6] J. Cleveland, Modular high-temperature gas-cooled reactor short-term thermal response to flow and reactivity transients, Nuclear technology, 91 (1990) 247-258.
[7] J.P. Gorton, N.R. Brown, Defining the performance envelope of reactivity-initiated accidents in a high-temperature gas-cooled reactor, Nuclear Engineering and Design, 370 (2020) 110865.
[8] C.G. Ghezzi, D. Schappel, G. Pastore, B.D. Wirth, N.R. Brown, Sensitivity Analysis applied to SiC Failure Probability in TRISO modeled with BISON, Submitted for review, (2022).
[9] C. Rabiti, A. Alfonsi, J. Cogliati, D. Mandelli, R. Kinoshita, S. Sen, C. Wang, P.W. Talbot, D.P. Maljovec, J. Chen, RAVEN user manual, Idaho National Lab.(INL), Idaho Falls, ID (United States), 2017.
[10] G. Strydom, A. Epiney, A. Alfonsi, C. Rabiti, Comparison of the PHISICS/RELAP5-3D ring and block model results for phase I of the OECD/NEA MHTGR-350 benchmark, Nuclear Technology, 193 (2016) 15-35.
[11] C. Lu, B.D. Hiscox, K.A. Terrani, N.R. Brown, Fully ceramic microencapsulated fuel in prismatic high temperature gas-cooled reactors: analysis of reactor performance and safety characteristics, Annals of Nuclear Energy, 114 (2018) 277-287.
[12] C. Lu, N.R. Brown, Fully ceramic microencapsulated fuel in prismatic high-temperature gas-cooled reactors: Design basis accidents and fuel cycle cost, Nuclear Engineering and Design, 347 (2019) 108-121.
[13] C. Lu, T. Koyanagi, Y. Katoh, G. Strydom, K.A. Terrani, N.R. Brown, Fully Ceramic Microencapsulated fuel in prismatic high-temperature gas-cooled reactors: Sensitivity of reactor behavior during design basis accidents to fuel properties and the potential impact of the SiC defect annealing process, Nuclear Engineering and Design, 345 (2019) 125-147.
[14] P. Williams, F. Silady, T. Dunn, R. Noren, D. McEachern, D. Dilling, J. Berkoe, F. Homan, L. Mears, S. Penfield Jr, MHTGR development in the United States, Progress in Nuclear Energy, 28 (1994) 265-346.
[15] E.M. Duchnowski, R.F. Kile, L.L. Snead, J.R. Trelewicz, N.R. Brown, Reactor performance and safety characteristics of two-phase composite moderator concepts for modular high temperature gas cooled reactors, Nuclear Engineering and Design, 368 (2020) 110824.
[16] J.D. Hales, R.L. Williamson, S.R. Novascone, G. Pastore, B.W. Spencer, D.S. Stafford, K.A. Gamble, D.M. Perez, W. Liu, BISON theory manual the equations behind nuclear fuel analysis, Idaho National Lab.(INL), Idaho Falls, ID (United States), 2016.
[17] J.D. Hales, R.L. Williamson, S.R. Novascone, D.M. Perez, B.W. Spencer, G. Pastore, Multidimensional multiphysics simulation of TRISO particle fuel, Journal of Nuclear Materials, 443 (2013) 531-543.

[18] P. Hosemann, J.N. Martos, D. Frazer, G. Vasudevamurthy, T.S. Byun, J.D. Hunn, B.C. Jolly, K. Terrani, M. Okuniewski, Mechanical characteristics of SiC coating layer in TRISO fuel particles, Journal of nuclear materials, 442 (2013) 133-142.
[19] L.L. Snead, T. Nozawa, Y. Katoh, T.-S. Byun, S. Kondo, D.A. Petti, Handbook of SiC properties for fuel performance modeling, Journal of nuclear materials, 371 (2007) 329-377.
[20] C. Lu, R. Danzer, F. Fischer, Fracture statistics of brittle materials: Weibull or normal distribution, Physical review. E, Statistical, nonlinear, and soft matter physics, 65 (2002) 067102.
[21] T.S. Byun, E. Lara-Curzio, R.A. Lowden, L.L. Snead, Y. Katoh, Miniaturized fracture stress tests for thin-walled tubular SiC specimens, Journal of nuclear materials, 367 (2007) 653-658.
[22] T.S. Byun, J.D. Hunn, J.H. Miller, L.L. Snead, J.W. Kim, Evaluation of fracture stress for the SiC layer of TRISO-coated fuel particles using a modified crush test method, International Journal of Applied Ceramic Technology, 7 (2010) 327-337.
[23] J.D. Hunn, T.S. Byun, J.H. Miller, Fabrication and Characterization of Sixteen SiC Variants Deposited on the Same IPyC Substrate for Fracture Strength Testing, ORNL/TM-2009/324, (2009).
[24] S.G. Hong, T.S. Byun, R.A. Lowden, L.L. Snead, Y. Katoh, Evaluation of the fracture strength for silicon carbide layers in the tri-isotropic-coated fuel particle, Journal of the American Ceramic Society, 90 (2007) 184-191.
[25] I.y.M. Sobol, On sensitivity estimation for nonlinear mathematical models, Matematicheskoe modelirovanie, 2 (1990) 112-118.
[26] A. Saltelli, P. Annoni, I. Azzini, F. Campolongo, M. Ratto, S. Tarantola, Variance based sensitivity analysis of model output. Design and estimator for the total sensitivity index, Computer physics communications, 181 (2010) 259-270.
[27] I.y.M. Sobol, On the distribution of points in a cube and the approximate evaluation of integrals, Zhurnal Vychislitel'noi Matematiki i Matematicheskoi Fiziki, 7 (1967) 784-802.
[28] I.M. Sobol, Uniformly distributed sequences with an additional uniform property, USSR Computational Mathematics and Mathematical Physics, 16 (1976) 236-242.
[29] I.M. Sobol′, Global sensitivity indices for nonlinear mathematical models and their Monte Carlo estimates, Mathematics and Computers in Simulation, 55 (2001) 271-280.
[30] J. Herman, W. Usher, SALib: an open-source Python library for sensitivity analysis, Journal of Open Source Software, 2 (2017) 97.
[31] A. Saltelli, Making best use of model evaluations to compute sensitivity indices, Computer physics communications, 145 (2002) 280-297.
[32] A. Saltelli, M. Ratto, T. Andres, F. Campolongo, J. Cariboni, D. Gatelli, M. Saisana, S. Tarantola, Introduction to sensitivity analysis, Global sensitivity analysis. The primer, (2008) 1-51.
[33] Z. Aly, A. Casagranda, G. Pastore, N.R. Brown, Variance-based sensitivity analysis applied to hydrogen migration and redistribution model in Bison. Part I: Simulation of historical experiments, Journal of Nuclear Materials, 524 (2019) 90-100.
[34] Z. Aly, A. Casagranda, G. Pastore, N.R. Brown, Variance-based sensitivity analysis applied to the hydrogen migration and redistribution model in Bison. Part II: Uncertainty quantification and optimization, Journal of Nuclear Materials, 523 (2019) 478-489.

[35] N. Rohbeck, P. Xiao, Evaluation of the mechanical performance of silicon carbide in TRISO fuel at high temperatures, Nuclear Engineering and Design, 306 (2016) 52-58.
[36] Fuel Performance and Fission Product Behaviour in Gas-Cooled Reactors, INTERNATIONAL ATOMIC ENERGY AGENCY, Vienna, 1997.
[37] M.N. Cinbiz, T. Koyanagi, G. Singh, Y. Katoh, K.A. Terrani, N.R. Brown, Failure behavior of SiC/SiC composite tubes under strain rates similar to the pellet-cladding mechanical interaction phase of reactivity-initiated accidents, Journal of Nuclear Materials, 514 (2019) 66-73.
[38] A.V. Samant, W.L. Zhou, P. Pirouz, Effect of test temperature and strain rate on the yield stress of monocrystalline 6H-SiC, physica status solidi (a), 166 (1998) 155-169.
[39] J. Lankford, Mechanisms responsible for strain-rate-dependent compressive strength in ceramic materials, Journal of the American Ceramic Society, 64 (1981) C-33-C-34.
[40] N. Lissart, J. Lamon, Statistical analysis of failure of SiC fibres in the presence of bimodal flaw populations, Journal of materials science, 32 (1997) 6107-6117.
[41] B.V. Cockeram, Fracture strength of plate and tubular forms of monolithic silicon carbide produced by chemical vapor deposition, Journal of the American Ceramic Society, 85 (2002) 603-610.
[42] R. Belles, W. Poore III, N.R. Brown, G.F. Flanagan, M. Holbrook, W. Moe, T. Sofu, Proposed Adaptation of the Standard Review Plan NUREG-0800, Chapter 4 (Reactor) for Sodium-Cooled Fast Reactors and Modular High-Temperature Gas-Cooled Reactors, Oak Ridge National Lab.(ORNL), Oak Ridge, TN (United States), 2017.
[43] R.O. Scarlat, M.R. Laufer, E.D. Blandford, N. Zweibaum, D.L. Krumwiede, A.T. Cisneros, C. Andreades, C.W. Forsberg, E. Greenspan, L.-W. Hu, Design and licensing strategies for the fluoride-salt-cooled, high-temperature reactor (FHR) technology, Progress in Nuclear Energy, 77 (2014) 406-420.